Tunneling of a few strongly repulsive hard-sphere bosons in an optical lattice with tight external harmonic confinement: A quantum Monte Carlo investigation in continuous space

Asaad R. Sakhel,[1] Jonathan L. Dubois,[2] and Roger R. Sakhel[3]
[1]*Al-Balqa Applied University, Faculty of Engineering Technology, Basic Sciences Department, Amman 11134, Jordan*
[2]*Lawrence Livermore National Laboratory, 7000 East Ave, L-415, Livermore California 94550, USA*
[3]*Department of Basic Sciences, Faculty of Science and Information Technology, Al-Isra University, Amman 11622, Jordan*
(Received 31 October 2009; published 7 April 2010)

The effect of strongly repulsive interactions on the tunneling amplitude of hard-sphere (HS) bosons confined in a simple cubic optical lattice plus tight external harmonic confinement in continuous space is investigated. The quantum variational Monte Carlo (VMC) and the variational path integral (VPI) Monte Carlo techniques are used at zero temperature. The effects of the lattice spacing on the tunneling amplitude are also considered. The occupancies of the lattice sites as a function of the repulsion between the bosons are further revealed. Our chief result is that for a small number of bosons ($N = 8$) the overlap of the wave functions in neighboring wells practically does not change with an increase of the repulsive interactions and changes only minimally for a larger number of particles ($N = 40$). The tunneling amplitude rises with a reduction in the lattice spacing. In addition, the occupancy of the center of the trap decreases in favor of a rise in the occupancy of the lattice sites at the edges of the trap with increasing HS repulsion. Further, it was found that the energy per particle at certain optical-lattice barrier heights is insensitive to the number of particles and variations in the HS diameter of the bosons. In order to support our results, we compare the VMC results with corresponding VPI results.

DOI: 10.1103/PhysRevA.81.043603 PACS number(s): 67.85.−d, 03.75.Lm

I. INTRODUCTION

The tunneling of bosons [1–6] as well as that of fermions [7] in optical lattices has drawn considerable interest in the past few years. This is due to its connection to superfluidity (SF) [8] and its analogy to Josephson tunneling in quantum devices [9]. Particularly the role of interparticle interactions in determining the tunneling amplitude has only been given few investigations [2,3,6,10] and to the best of our knowledge. Tunneling in multiple wells has also been given consideration [11].

In simple elementary terms, the quantum tunneling of a particle through a potential barrier, such as in an optical lattice, can occur when its total energy E is less than the height of the barrier V_0. The particle is described by a wave packet which can penetrate the barrier with a finite probability. As a result, an overlap between two wave functions at both sides of the barrier provides a measure for the tunneling amplitude of the particle. Potential barriers of this sort have been realized in quantum devices [9] that make use of Josephson tunneling [12] and in the recently achieved optical traps [13].

When there is more than a single atom in the potential well, the mechanism of quantum tunneling is very much determined by the strength of the interatomic interactions. In the strongly interacting regime, correlated tunneling occurs [3,10] where atoms tunnel in pairs and which competes with single-particle tunneling. One of the most important properties of single-particle tunneling in optical lattices is that it is a signature of a SF state [8] and, if absent, of a Mott-insulator (MI) state [6,14]. Pair superfluidity (PSF) has also been recently discussed [15,16]. In an MI state, the particles are unable to superflow but still able to hop from one well to the other. This is via the correlated hopping mechanism which in this article might be signalled by an overlap of the wave functions in neighboring wells in the strongly interacting regime. In fact it was Fölling *et al.* [3] who showed experimentally that strong interactions suppress single-particle tunneling such that second-order correlated tunneling is then the dominant dynamical effect. An SF state is quite the opposite, where considerable single-particle tunneling and phase coherence are observed.

In this article, we chiefly investigate the effects of strongly repulsive interactions on the tunneling amplitude of bosons in an inhomogeneous system confined by a tight combined harmonic optical lattice. The external harmonic trap is spherically symmetric. It introduces an inhomogeneity in the atomic density distributions and restricts the motion of the bosons within the confining volume. Investigations on bosons confined in an optical lattice plus external trap have been conducted before as well [17–20]. We use two different ways for measuring the tunneling amplitude. One way is by evaluating the overlap integral of wave functions in neighboring wells, obtained from the integrated optical densities. The other is by evaluating an exchange integral [6] in order to obtain the single-particle tunneling amplitude. We use quantum variational Monte Carlo (VMC) and variational path integral (VPI) Monte Carlo techniques in continuous space at zero Kelvin. To the best of our knowledge, previous work did not consider the effects of inhomogeneiety on the tunneling amplitude of strongly repulsive lattice bosons, particularly by using Monte Carlo techniques in continuous space.

To this end, the tunneling amplitude of bosons in optical lattices has been investigated chiefly as a function of the optical-lattice barrier height V_0 [8,21] and number of particles [6]. An investigation most relevant to our work is that of Shams and Glyde [8]. They evaluated the BEC density and SF fraction of hard-sphere (HS) bosons confined in an external periodic potential using path-integral Monte Carlo (PIMC) methods in order to shed further light on the connection between BEC and SF. In part, they investigated the hopping parameter as a function of V_0 and showed that if V_0 is increased sufficiently, the condensate is localized into islands inside the potential wells suppressing superflow substantially. Further, they found that their external potential suppresses the SF fraction at all temperatures.

In our investigation, a key point is that in contrast to Shams and Glyde, V_0 is kept fixed while the repulsive interactions between the bosons are varied. Further, the effects of these interactions on atom correlations, optical density (OD), occupancy of lattice sites, onsite interaction energies, and the total energies are explored. In addition, the effects due to lattice spacing and number of particles are further revealed. As outlined in the method section, the bosons are represented by hard spheres of diameter a_c whose repulsive interactions can be modified by changing a_c, thereby mimicking the Feshbach resonance technique [22]. In one part of our work, we further compare between the roles of the optical-lattice barrier height V_0 and the HS repulsion (a_c) in the reduction of the tunneling amplitude.

Our chief result is that, for a small number of bosons, the overlap of wave functions in neighboring potential wells practically does not change with increasing HS repulsion and changes only minimally for $N = 40$. The localized wave functions in the potential wells do not broaden with an increase in a_c, in contrast to the case of HS bosons in pure harmonic traps [23,24]. In the latter, the width of the spacial many-body wave function extends to several trap lengths, whereas in our case, the wave function in each well extends only slightly beyond two trap lengths even at large repulsion. We thus have evidence to suggest that the optical lattice barriers prevent the wave functions in each well from expanding to a comparable extent as in pure harmonic traps. We further found that the energy per particle is relatively insensitive to the number of particles N and variations in a_c as compared to HS bosons in pure harmonic traps [23,24] and that the tunneling amplitude increases with the reduction of the lattice spacing. It is further found that increasing V_0 while keeping a_c fixed reduces the tunneling amplitude substantially as compared to the opposite case of changing a_c and keeping V_0 fixed, which hardly allows a reduction in the tunneling amplitude. Using the Wannier form [Eq. (4) below], we find that our wave function is sufficiently delocalized that it would seem most likely to describe a SF phase. In order to provide further support to our findings, we compare our VMC results with the corresponding VPI results.

Previous theoretical work on optical lattices is abundant, particularly the SF-to-MI transition [6,14,18,25–29], and coherent matter waves [30,31] have been investigated extensively. Other investigations included supersolidity [32,33], multicomponent systems [34,35], vortices [36], solitons [37,38], and p-h excitations in MIs [14].

Various techniques and methods have been used to investigate bosons, fermions, or mixtures of them in optical lattices: the Bose-Hubbard model [6,17,18,28,39] as well as the Fermi-Hubbard model [40,41] in conjunction with Monte Carlo techniques [18,28,40], and particularly diagrammatic Monte Carlo [41] and the worm algorithm [42,43] have been applied extensively. Other important techniques such as the Gross-Pitaevskii equation (GPE) [2,37], variational approaches [6,27,37], density matrix renormalization group [31], and path integral approaches [7] have also been used. Most of the above methods use a discrete space approach, whereas we evaluate the properties in continuous space.

The organization of the present article is as follows: In Sec. II we outline the methods used to evaluate the properties of the systems. Section III is devoted to the results of the present work. In Sec. IV we discuss the effect of the optical-lattice barrier height on the tunneling amplitude. Finally, in Sec. V we discuss our results and present our conclusions.

II. METHOD

We thus consider N bosons on a combined harmonic optical cubic lattice (CHOCL). It consists of a $3D^{al}$ simple cubic (sc) lattice of $N_L = 3 \times 3 \times 3$ sites embedded in a tight, external, and spherically symmetric harmonic trap of frequency $\omega_{\rm ho}$ and trap length $a_{\rm ho} = \sqrt{\hbar/m\omega_{\rm ho}}$. Here m is the mass of the bosons and $\hbar$ is Planck's constant. The lattice spacing is given by $d = \pi/k$, where k is the wave vector of the laser light. The bosons are modeled by hard spheres of diameter a_c and their interactions, $V_{\rm int}(r)$, are represented by a hard-core potential of diameter a_c given by

$$V_{\rm int}(r) = \begin{cases} \infty & : \quad r \leqslant a_c \\ 0 & : \quad r > a_c \end{cases}, \tag{1}$$

where r is the distance between a pair of bosons. In the low-energy limit, the scattering between the bosons is purely s wave with scattering length a_s. In this limit, a_s equals a_c [23,24] and the repulsive interactions between the bosons are modified by changing a_c. Within this framework then, the tunneling amplitude J and the rest of the properties are measured as functions of a_c.

To set the stage, then, we first define the Hamiltonian, and the trial wave function. Second, and as mentioned in the Introduction, the tunneling amplitude is measured in two ways:

1. By an overlap integral $I_{\rm overlap}$ of two wave functions in neighboring wells centered at positions $\mathbf{R}_n$ and $\mathbf{R}_{n+1}$ and are measured from the center of the trap, where n is an arbitrary integer. Here $n \equiv (pqr)$ are site indices with locations $\mathbf{R}_n = (p\hat{\mathbf{i}} + q\hat{\mathbf{j}} + r\hat{\mathbf{k}})$ in units of the lattice spacing d. By evaluating the overlap integral, the purpose is just to obtain a qualitative measure for the tunneling amplitude.

2. By the single-particle tunneling amplitude which is an exchange integral $\langle n|H|n+1\rangle$ between two sites n and $n+1$, where H is the Hamiltonian.

(Alternatively, the overlap integral of the single-particle densities at all lattice sites with the optical lattice potential is presented as a third measure for the tunneling amplitude, but here into the potential barriers.) Third, the average onsite interaction energy $\langle U_n\rangle$ and the average occupation number per lattice site $\langle N_{pqr}\rangle$ at position $\mathbf{R}_{[n\equiv(pqr)]}$ are further defined. These are evaluated using VMC and VPI. We do not explain the VMC and VPI methods here as they can be found in the abundant literature [23,44–46].

A. Hamiltonian

The Hamiltonian for our systems is given by

$$H = -\frac{\hbar^2}{2m}\sum_{i=1}^{N}\nabla_i^2 + \sum_{i=1}^{N}[V_{\rm ho}(\mathbf{r}_i) + V_{\rm opt}(\mathbf{r}_i)] + \sum_{i<j} V_{\rm int}(r_{ij}), \tag{2}$$

where $V_{\rm ho}(\mathbf{r}_i) = \frac{1}{2}m\omega_{\rm ho}^2 r_i^2$ is an external harmonic trapping potential with $\mathbf{r}_i \equiv (x_i, y_i, z_i)$ representing a single particle position, m the mass of the bosons, $V_{\rm int}(r_{ij})$ with

$r_{ij} = |\mathbf{r}_i - \mathbf{r}_j|$ the pair-interaction potential Eq. (1) above, and

$$V_{\rm opt}(\mathbf{r}_i) = V_0\,[\sin^2(kx_i) + \sin^2(ky_i) + \sin^2(kz_i)], \quad (3)$$

is the optical lattice potential [1,6] with V_0 the optical-lattice barrier height. Essentially, $V_{\rm opt}(\mathbf{r}_i = \mathbf{R}_n) = 0$ at the lattice-site positions $\mathbf{R}_n$ which are the locations of the potential-well minima of Eq. (3). That is, $V_{\rm opt}(\mathbf{R}_n) = V_0[\sin^2(p\pi) + \sin^2(q\pi) + \sin^2(r\pi)] = 0$, where $\mathbf{k}\cdot\mathbf{R}_n = (\text{integer}) \times \pi$. Thus the lattice-site positions are implied in $V_{\rm opt}(\mathbf{r}_i)$ by its very construction. Experimentally, the optical lattice potential is obtained from a superposition of three pairs of mutually perpendicular, counterpropagating laser beams of intensity proportional to V_0. For an sc lattice, V_0 must be the same for each direction. In this article, we write energy and length in units of the trap, $\hbar\omega_{\rm ho}$ and $a_{\rm ho} = \sqrt{\hbar/m\omega_{\rm ho}}$, respectively.

B. Trial wave function

The many-body trial wave function is given by

$$\Psi(\{\mathbf{r}\},\{\mathbf{R}\}) = \prod_{i=1}^{N} \exp\left(-\alpha r_i^2\right)\psi(\mathbf{r}_i,\{\mathbf{R}\}) \prod_{i<j} f(|\mathbf{r}_i - \mathbf{r}_j|), \quad (4)$$

with $\psi(\mathbf{r}_i,\{\mathbf{R}\})$ a Wannier-like function defined as

$$\psi(\mathbf{r}_i,\{\mathbf{R}\}) = \sum_{n=0}^{N_L} \phi(\mathbf{r}_i,\mathbf{R}_n), \quad (5)$$

where $\{\mathbf{r}\} \equiv \{\mathbf{r}_1,\mathbf{r}_2,\ldots,\mathbf{r}_N\}$ is a set of spatial vectors describing the positions of the bosons from the center of the trap, $\{\mathbf{R}\} \equiv \{\mathbf{R}_1,\mathbf{R}_2,\ldots,\mathbf{R}_{N_L}\}$ is a set of vectors describing the positions of the lattice potential minima on the $3\times3\times3$ cubic lattice cage considered, and α is a variational parameter signaling the strength of the external harmonic confinement. Essentially, α is the inverse overall width of the total wave function of the system in the CHOCL. Further, α controls the volume of the external harmonic confinement and, therefore, the number of lattice sites to be occupied away from the center of the trap. Equation (5) is constructed in a manner similar to that of Jin *et al.* [35] in that we sum over a number of localized single-particle wave functions $\phi(\mathbf{r}_i,\mathbf{R}_n)$ centered in the optical lattice wells, each at $\mathbf{R}_n$. As for $\phi(\mathbf{r}_i,\mathbf{R}_n)$, it is constructed similarly to the wave function used by Li *et al.* [6] and is given by:

$$\begin{aligned}\phi(\mathbf{r}_i,\mathbf{R}_n) = \exp[-\beta(\mathbf{r}_i - \mathbf{R}_n)^2][1 + \gamma(x_i - X_n)^2 \\ - \sigma(x_i - X_n)^4][1 + \gamma(y_i - Y_n)^2 - \sigma(y_i - Y_n)^4] \\ \times [1 + \gamma(z_i - Z_n)^2 - \sigma(z_i - Z_n)^4], \end{aligned} \quad (6)$$

where β, γ, and σ are further variational parameters in addition to α. The onsite repulsion is partly controlled by the local density $|\phi(\mathbf{r}_i,\mathbf{R}_n)|^2$ via the variational parameter β in Eq. (6), which confines the particles at each lattice site (n). The interactions in the trial wave function are taken into account by the usual HS Jastrow function [23,24]:

$$f(r_{ij}) = \begin{cases} 0 & : \quad r_{ij} \leqslant a_c \\ 1 - \frac{a_c}{r_{ij}} & : \quad r_{ij} > a_c \end{cases}, \quad (7)$$

where r_{ij} is the distance between a pair of bosons. The Jastrow function Eq. (7) is the zero-momentum limit of the solution to the two-body Schrödinger equation in the low-energy and long-wavelength limit:

$$\lim_{\mathbf{k}\to0} \psi_{\mathbf{k}}^{(+)}(\mathbf{r}) = \lim_{\mathbf{k}\to0} \frac{\sin(kr + \delta_0)}{kr} = 1 - \frac{a_s}{r},$$

since $\delta_0 = -ka_s$ is the phase shift from standard scattering theory [47] by using a contact potential $V(r) = g\delta(r)$, where $g = 4\pi\hbar^2 a_s/m$. This Jastrow function keeps the bosons away from each other at a certain average distance and prevents them from touching each other. One could also have used, for example, $f(r) = 1 - (a/r)^\nu$, where ν is some adjustable parameter. If $\nu > 1$ then the Jastrow function runs "faster" to 1, i.e., $f(r)$ becomes 1 at a shorter distance r than in Eq. (7). As a result, the bosons would approach each other further.

The VMC wave function (4) is optimized by minimizing the average energy with Powell's technique [48] employed in a previous publication [49]. The ground-state configuration is achieved when all the particles are distributed symmetrically in the spherical coordination shells around the center of the trap, and the overall boson-boson repulsion is minimal. Once the trial function Eq. (4) has been optimized, it is plugged into the VPI code as a starting wave function. The same properties are then evaluated as those using VMC.

C. Optical density definition

In this work, the optical column density is measured, and as follows. First, for each MC configuration of particles, labeled c, we define a 2D particle density $n_{2D,c}(x,y)$ given by

$$n_{2D,c}(x,y) = \int_{-\infty}^{+\infty} |\Psi_c(x,y,z)|^2 dz. \quad (8)$$

where $|\Psi_c|^2$ is the total density of a configuration c. $n_{2D,c}(x,y)$ is obtained by binning particles in square bins in the xy plane on a grid over several Monte Carlo steps. The configurational average of this density is then evaluated by summing (8) over all configurations and dividing by the number of configurations P:

$$\langle n_{2D}(x,y)\rangle = \sum_c n_{2D,c}(x,y)/P. \quad (9)$$

The 1D optical density (OD) is obtained by taking a slice of $\langle n_{2D}(x,y)\rangle$ along one of the axes, that is

$$n_{1D}(x) = \langle n_{2D}(x,y=0)\rangle. \quad (10)$$

D. Tunneling

The tunneling amplitude in this work is now measured in the previously outlined two ways at the beginning of Sec. II. We discuss both methods now.

1. Overlap of wave functions in neighboring wells

A qualitative measure for the overlap of the wave functions is evaluated, for simplicity, from trial-density functions fitted to slices of the integrated optical densities (OD) along one axis. For this purpose, we choose the trial-density functions similar to the one-dimensional (1D) version of Eq. (6) with an

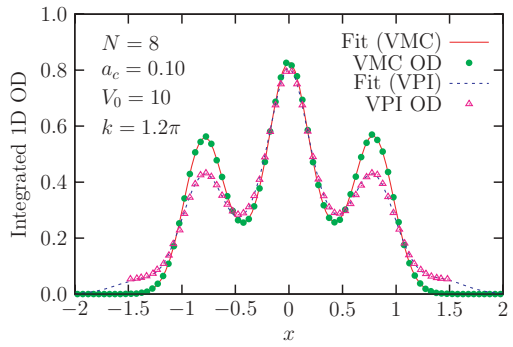

FIG. 1. (Color online) Fits using the forms (11) and (12) to 1D VMC and VPI integrated OD slices along the x axis [$n_{1D}(x)$, Eq. (10)] for a system of $N = 8$, $V_0 = 10$, $a_c = 0.10$, and $k = 1.2\pi$ in a CHOCL of $3 \times 3 \times 3$ lattice sites. VMC fit (dotted line), VMC OD (solid circles), VPI fit (dashed line), and VPI OD (open triangles). The sum of squares for both fits is $\chi^2 = 3.41 \times 10^{-4}$ for VMC and 7.41×10^{-4} for VPI, respectively. All lengths and energies are in units of the trap $a_{\rm ho} = \sqrt{\hbar/m\omega_{\rm ho}}$ and $\hbar\omega_{\rm ho}$, respectively. The x and a_c are in units of $a_{\rm ho}$, k is in units of $a_{\rm ho}^{-1}$, and V_0 is in units of $\hbar\omega_{\rm ho}$. The 1D OD is in units of $a_{\rm ho}^{-1}$.

additional amplitude factor A_n, that is

$$|\phi_{\rm fit}(x,X_n)|^2 = A_n \exp[-\beta_n(x-X_n)^2] \times |1+\gamma_n(x-X_n)^2+\sigma_n(x-X_n)^4|. \quad (11)$$

The absolute value is considered to make sure we do not run into negative densities. An example of such a fit is shown in Fig. 1 above displaying the VMC fit (dotted line), VMC OD (solid circles), VPI fit (dashed line), and VPI OD (open triangles). Here, the fitting function is

$$F(x;X_1,X_2,X_3) = \sum_{n=1}^{3} |\phi_{\rm fit}(x,X_n)|^2, \quad (12)$$

having peaks centered at three potential minima X_1 (left), X_2 (center), and X_3 (right) and with three sets of fitting parameters A_n, β_n, γ_n, σ_n, and the latter X_n, where n runs from 1 to 3. In fact, the central position X_2 always turns out to be exactly zero as required. The sum of squares

$$\chi^2 = \sum_{i=1}^{p} \left\{ \sum_{n=1}^{3} [|\phi_{\rm fit}(x_i,X_n)|^2 - |\phi_{MC}(x_i,X_n)|^2] \right\}^2 \quad (13)$$

is minimized with respect to the above sets of fitting parameters. Here χ^2 is a sum over all p data points of the 1D integrated MC OD $[\sum_{n=1}^{3} |\phi_{MC}(x_i,X_n)|^2]$. By this minimization, we get values of $\chi^2 < 10^{-3}$, indicating a good fit. After optimization, the overlap integral

$$I_{\rm overlap} = \int_{-\infty}^{+\infty} \phi_{\rm fit}(x,X_1)\,\phi_{\rm fit}(x,X_2)\,dx + \int_{-\infty}^{+\infty} \phi_{\rm fit}(x,X_2)\,\phi_{\rm fit}(x,X_3)\,dx, \quad (14)$$

is then evaluated using a simple elementary numerical technique.

2. *Single particle tunneling*

One can describe the single-particle tunneling amplitude for strongly interacting systems using the well-known exchange integral [6]

$$J_n = \langle n|H|n+1\rangle = \int d^3r\,\phi_n(\mathbf{r}) \left[-\frac{\hbar^2}{2m}\nabla^2 + V(\mathbf{r})\right] \phi_{n+1}(\mathbf{r}), \quad (15)$$

where ϕ_n and ϕ_{n+1} are single-particle wave functions at sites n and $n+1$, and $V(\mathbf{r})$ a single-particle potential. In fact, it is anticipated that the single-particle wave function narrows as the HS repulsion rises, counteracting the effects of the broadening due to the Jastrow factor [Eq. (7)] as the number of particles is increased beyond a certain limit. Thus for one boson tunneling between two neighboring potential wells of indices n and $n+1$ and positions $\mathbf{R}_n$ and $\mathbf{R}_{n+1}$, respectively, J for each boson is given by Eq. (15). In order to incorporate the effects of the external trap into the tunneling amplitude, we use a slightly modified version of their J, namely the average

$$\left\langle J_{[\mathbf{R}_n \to \mathbf{R}_{n+1}]} \right\rangle = \int_{\langle MC \rangle} d^3r\, e^{-\alpha r^2} \phi(\mathbf{r},\mathbf{R}_n) \left[-\frac{\hbar^2}{2m}\nabla^2 + V(\mathbf{r})\right] \times e^{-\alpha r^2} \phi(\mathbf{r},\mathbf{R}_{n+1}), \quad (16)$$

where $\int_{\langle MC \rangle}$ stands for a MC configurational integral defined in Sec. III below. In Eq. (16) we have multiplied the wave function in each well by the factor $\exp(-\alpha r^2)$ representing the external harmonic trap. $V(\mathbf{r})$ is usually the periodic optical lattice potential, but in the present work, we superimpose a tight external trap, $V_{\rm ho}(\mathbf{r})$, on the optical lattice potential: $V(\mathbf{r}) = V_{\rm opt}(\mathbf{r}) + V_{\rm ho}(\mathbf{r})$. Thus, a basic feature in our work is to include the effects of a steeply varying external harmonic trap into our calculations. We evaluate the average of $\langle J \rangle$ for all N bosons between two chosen neighboring lattice sites $\mathbf{R}_n = (000)$ and $\mathbf{R}_{n+1} = (00-1)$. We consider only (000) and (00 −1) because (00 −1) alone is representative of the first nearest-neighbor family and the tunneling amplitude is symmetric around the trap center in the six directions.

E. Bosons-optical lattice overlap

A measure for the extent of the overlap between $[\phi(\mathbf{r}_i,\mathbf{R}_n)]^2$ and $V_{\rm opt}(\mathbf{r}_i)$ for all particles $i = 1$ to N and all lattice sites $n = 1$ to N_L is given by

$$\langle I_{\rm boson-OL} \rangle = \sum_{n=1}^{N_L} \int_{\langle MC \rangle} [e^{(-\alpha r^2)} \phi(\mathbf{r},\mathbf{R}_n)]^2\, V_{\rm opt}(\mathbf{r})\, d^3r, \quad (17)$$

where OL stands for optical lattice. Further, $\langle I_{\rm boson-OL} \rangle$ is an indirect measure of the total tunneling amplitude of the system into the optical lattice potential barriers. In this regard, we follow Giamarchi and Schultz [50] in constructing an overlap integral analogous to their Eq. (5.7).

F. Discrete onsite interaction energies

In order to further explore the single-particle response to the change in the HS repulsions, we evaluate the onsite interaction energies at individual lattice sites. Another goal

is to provide the onsite interaction for measuring zJ/U. The onsite interaction energy for a single particle at each lattice site (n) is evaluated following [6,51] as

$$\langle U_n \rangle = g \int_{\langle MC \rangle} e^{-4\alpha r^2} |\phi(\mathbf{r},\mathbf{R}_n)|^4 \, d^3r, \tag{18}$$

where

$$g = 4\pi\hbar^2 a_c/m, \tag{19}$$

with a_s replaced by a_c. Here the effects of the external trap are included via the factor $[\exp(-\alpha r^2)]^4$. In our calculations, we used $g = 4\pi a_c$ which is in trap units.

G. Occupancy of lattice sites

Another single-particle response is the average atom-number occupancy of each lattice site (n) evaluated via

$$\langle N_n \rangle = N \int_{\langle MC \rangle} e^{-2\alpha r^2} |\phi(\mathbf{r},\mathbf{R}_n)|^2 d^3r. \tag{20}$$

An alternative way to determine the occupancy of each lattice site is to divide the confining volume into equivalent cubic bins whose corners are sets of four lattice sites $\mathbf{R}_n$ and count the number of particles collected in each bin. We used this counting method to evaluate the VPI $\langle N_n \rangle$, whereas (20) to obtain the VMC $\langle N_n \rangle$.

H. Correlations between the bosons

The pair correlation function $g(r)$ is evaluated using VPI by binning pairs of particles in each r. The idea is to provide a measure for the strength of the boson-boson correlations and its dependency on the repulsive interactions in a tightly confining environment.

I. Numerics

The integrals (16)–(18) and (20) are evaluated using standard Monte Carlo integration [46]:

$$\int_{\langle MC \rangle} O(\mathbf{r}) d\mathbf{r} = \frac{1}{N} \sum_{i=1}^{N} \frac{1}{P} \sum_{c=1}^{P} \frac{O(\mathbf{r}_{ci})}{e^{-2\alpha r_{ci}^2} \sum_{n=1}^{N_L} |\phi(\mathbf{r}_{ci},\mathbf{R}_n)|^2}, \tag{21}$$

where c is a configurational index, i is a particle index, and P is the total number of VMC or VPI configurations $\{\mathbf{r}_{ci}\}$. We further sum over all N particles and divide by N to get the average for all particles. The denominator is a weight we used for all MC integrals. The sum (21) is conducted over a large number of configurations in order to get the MC cumulative average and to reduce the statistical error.

In VPI, each configuration consists of N particle positions along one chosen time slice. The integral (21) for each of the previous observables (16)–(18) and (20) is evaluated at the first and last time slices of the path, 1 and $2M$. (We use here the same notation as Ref. [44].) We then found it convenient to take the average of the two time slices, e.g., $\langle U_n \rangle \to (\langle U_n^{(1)} \rangle + \langle U_n^{(2M)} \rangle)/2$, where $\langle U_n^{(1)} \rangle$ is the average onsite interaction energy as evaluated by Eqs. (18) and (21) at slice 1 and similarly $\langle U_n^{(2M)} \rangle$ at slice $2M$. In that sense, the expectation values above are evaluated using the "mixed estimate" concept [44]. The optical densities Eqs. (9) and (10), however, are evaluated at the central slice of the path.

J. Energy

The VPI energy is evaluated via the "mixed estimate" [44] by taking the average of the energies at two time slices, $\langle E \rangle = (\langle E^{(1)} \rangle + \langle E^{(2M)} \rangle)/2$ where the first slice is 1 and the last $2M$, and

$$\langle E^{(1)} \rangle = \frac{1}{P} \sum_{c=1}^{P} \frac{\hat{H}\Psi(\{\mathbf{r}_c^{(1)}\},\{\mathbf{R}\})}{\Psi(\{\mathbf{r}_c^{(1)}\},\{\mathbf{R}\})} \tag{22}$$

$$\langle E^{(2M)} \rangle = \frac{1}{P} \sum_{c=1}^{P} \frac{\hat{H}\Psi(\{\mathbf{r}_c^{(2M)}\},\{\mathbf{R}\})}{\Psi(\{\mathbf{r}_c^{(2M)}\},\{\mathbf{R}\})}. \tag{23}$$

Here $\Psi(\{\mathbf{r}_c^{(1,2M)}\},\{\mathbf{R}\})$ is the same as Eq. (4), but with $\mathbf{r} = \mathbf{r}_c^{(1,2M)}$ labeled as the configuration of particles at time slice 1 or 2M, respectively. According to Cuervo *et al.* [44], it is possible to use the first as well as the last time slice for the mixed estimate.

We must also draw the attention of the reader to the fact that by using the trial wave function Eq. (4), we are not separating the energies into relative and center of mass motion, but we are measuring motions relative to the positions of the lattice sites $\{\mathbf{R}\}$ and $\mathbf{r}$ is measured relative to the center of the HO trap. The center of the HO trap coincides with the center of the cubic lattice. Our trial wave function does not allow center-of-mass motion.

K. Computational complexities

As much as VPI is an accurate method for the present determination of the properties of lattice bosons, using a number of particles exceeding $N = 8$, this method begins to constitute a heavy-computational and CPU-time-consuming technique. Particularly, for large optical potential barriers $V_0 \geqslant 10\hbar\omega_{\rm ho}$, the bosons take a very long CPU time to tunnel through the barriers in order to achieve a symmetric OD distribution inside the whole trap. We therefore limited the number of particles to $N = 8$ when using VPI. On the other hand, the less accurate VMC method allows the bosons to diffuse quickly through the barriers providing a computationally cheap and fast technique to investigate qualitatively the properties of bosons in optical lattices. Our aim is, however, not to present methods but to concentrate on the physics of quantum tunneling.

L. Alternative VMC trial function

In order to test the validity of using a Gaussian $[\exp(-\alpha r^2)]$ in our trial wave function Eq. (4), we calculated the optical densities for $N = 8$, $V_0 = 10$, and $k = \pi$ using a slightly modified version of our trial wave function:

$$\Psi(\{\mathbf{r}\},\{\mathbf{R}\}) = \prod_{i=1}^{N} \exp\left(-\alpha\, r_i^2 - \epsilon\, r_i^4\right) \psi(\mathbf{r}_i,\{\mathbf{R}\}) \times \prod_{i<j} f(|\mathbf{r}_i - \mathbf{r}_j|), \tag{24}$$

with an additional parameter ϵ added to the previous set of variational parameters. Figure 2 displays the 1D density slices $n_{1D}(x)$ evaluated via Eq. (24) at the indicated values of a_c. The

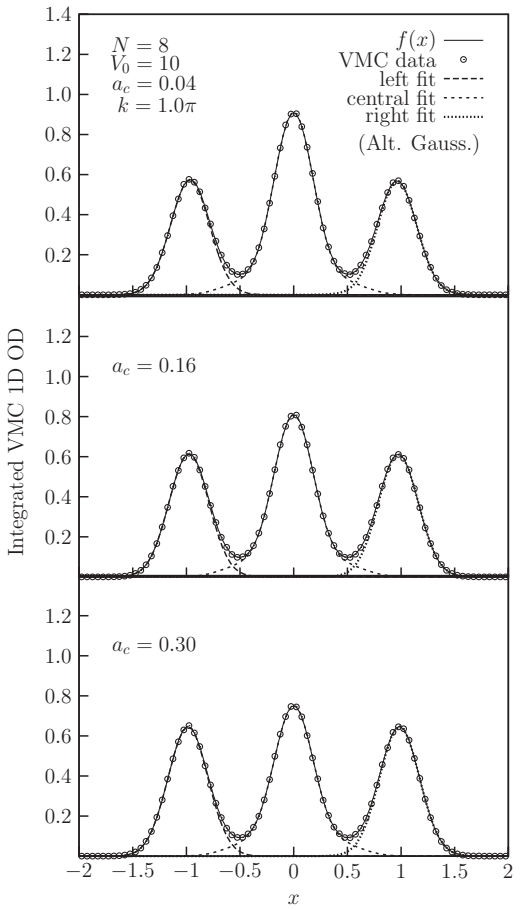

FIG. 2. Integrated one-dimensional (1D) OD slices $n_{1D}(x)$ [Eq. (10)] evaluated using the alternative Gaussian in Eq. (24) (Alt. Gauss). The system is a HS Bose gas of $N = 8$, $V_0 = 10$, and $k = \pi$, in a CHOCL of $3 \times 3 \times 3$ sites. Solid line: fitting function $f(x) = F(x;X_1,X_2,X_3)$ [Eq. (12)], open circles: VMC data, thick dashed line: left fit $|\phi_{\rm fit}(x,X_1)|^2$, thin dashed line: central fit $|\phi_{\rm fit}(x,X_2 = 0)|^2$, dotted line: right fit $|\phi_{\rm fit}(x,X_3)|^2$. From top to bottom, $a_c = 0.04$, 0.16, and 0.30. The VMC 1D OD and k are in units of $a_{\rm ho}^{-1}$, V_0 is in units of $\hbar\omega_{\rm ho}$, and x and a_c are in units of $a_{\rm ho}$. The fits $|\phi_{\rm fit}(x,X_3)|^2$ (with $i = 1,2$, or 3) and $f(x)$ are in units of $a_{\rm ho}^{-1}$.

system is a HS Bose gas of $N = 8$, $V_0 = 10$, and $k = \pi$, in a CHOCL of $3 \times 3 \times 3$ lattice sites. Solid line: fitting function $f(x) = F(x;X_1,X_2,X_3)$ [Eq. (12)]; open circles: VMC data; dashed line: left fit $|\phi_{\rm fit}(x,X_1)|^2$; thin dashed line: central fit $|\phi_{\rm fit}(x,X_2 = 0|^2$; dotted line: right fit $|\phi_{\rm fit}(x,X_2)|^2$.

As one can see, the wave functions in each well do not broaden with increasing a_c, the central peak loses amplitude with increasing a_c, and the peaks at the edges gain amplitude. The upcoming conclusions of the article are not qualitatively changed by this new calculation. As we will see below, the differences between Figs. 2 and a comparable Fig. 24 are substantial. The overlap of the wave function in neighboring wells is significantly reduced in Fig. 2 as compared to Fig. 24, nevertheless, the qualitativeness of the results is the same in both figures.

A further comment on the results in Fig. 2 is in order here. VMC is very much dependent on the form of the trial wave function used. VPI, however, is independent of the initial wave function used. Whatever form for the trial wave function is employed, VPI always reaches the same result. In VMC, it is difficult to find the exact trial wave function that would lead us to the optimal ground-state solution. Nevertheless, we show that our trial wave function is of a good quality as it gives results very close to the VPI results.

M. Units

We emphasize again that all lengths and energies are measured in units of the trap, $a_{\rm ho} = \sqrt{\hbar/m\omega_{\rm ho}}$ and $\hbar\omega_{\rm ho}$, respectively. That is, we write $(x,y,z) \to (x/a_{\rm ho}, y/a_{\rm ho}, z/a_{\rm ho})$ and $\langle E\rangle \to \langle E\rangle/\hbar\omega_{\rm ho}$. Similarly, $\langle J_{[\mathbf{R}_n\to\mathbf{R}_{n+1}]}\rangle$, $\langle I_{\rm boson-OL}\rangle$, and $\langle U_n\rangle$ are rewritten in units of $\hbar\omega_{\rm ho}$. The densities $\langle n_{2D}(x,y)\rangle$ and $n_{1D}(x)$ are in units of $a_{\rm ho}^{-2}$ and $a_{\rm ho}^{-1}$, respectively, and the wave vector k is in units of $a_{\rm ho}^{-1}$. The overlap integral $I_{\rm overlap}$ is unitless since $\phi_{\rm fit}(x,X_i)$ in Eq. (14) is in units of $a_{\rm ho}^{-1/2}$. From now on, these units are used consistently in all the upcoming figures and interpretations of results.

III. RESULTS

In what follows, we present the results of our calculations. We particularly focus on the effect of interactions on the tunneling amplitude $\propto I_{\rm overlap}$. We further explore the effect of a_c on the onsite interaction energies $\langle U_n\rangle$, energy per particle $\langle E\rangle/N$, the occupancy of lattice sites $\langle N_n\rangle$, the overlap of the bosons with the OL potential, the correlations $g(r)$, and the OD. As mentioned before, we compare our VMC results with corresponding VPI results.

A. Tunneling

$I_{\rm overlap}$ is now displayed as a function of a_c. Figure 3 displays the VPI results for systems of $N = 8$ and $V_0 = 10$ in a CHOCL of $3 \times 3 \times 3$ lattice sites with $k = \pi$ (open circles), $k = 1.2\pi$ (open triangles) and $k = 1.4\pi$ (open diamonds). The VMC results are displayed similarly but with solid labels.

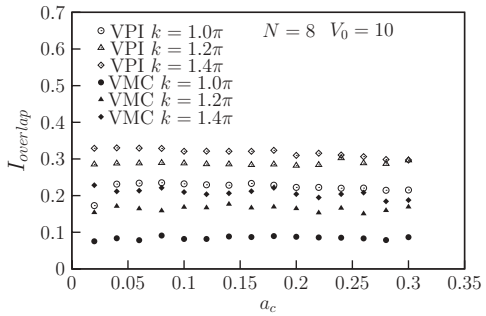

FIG. 3. Tunneling amplitude $\propto I_{\rm overlap}$ [Eq. (14)] vs. the hard-sphere (HS) diameter a_c, obtained from fits to 1D VPI and VMC optical density slices such as those in Fig. 2. The system is a HS Bose gas of $N = 8$ and $V_0 = 10$ in a CHOCL of $3 \times 3 \times 3$ sites. VPI results: $k = \pi$ (open circles); $k = 1.2\pi$ (open triangles); $k = 1.4\pi$ (open diamonds). The corresponding solid legends are for the VMC results. Lengths are in units of the trap $a_{\rm ho} = \sqrt{\hbar/m\omega_{\rm ho}}$. The $I_{\rm overlap}$ is unitless, k is in units of $a_{\rm ho}^{-1}$, V_0 is in units of $\hbar\omega_{\rm ho}$, and a_c is in units of $a_{\rm ho}$.

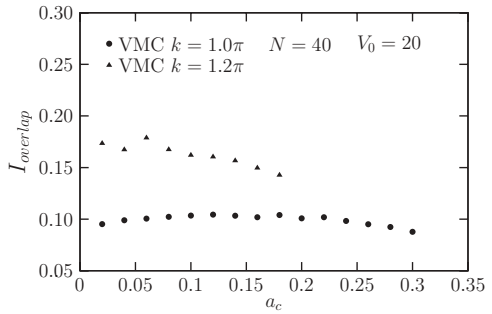

FIG. 4. As in Fig. 3; but using VMC for $N = 40$, $V_0 = 20$ and the indicated values of k. The I_{overlap} is unitless, k is in units of a_{ho}^{-1}, V_0 is in units of $\hbar\omega_{\text{ho}}$, and a_c is in units of a_{ho}.

For these values of N and V_0, I_{overlap} shows a very weak response to the effects of increasing a_c, since it seems to remain practically constant. As k is increased, I_{overlap} rises indicating a profound effect of the lattice spacing $d = \pi/k$ on the tunneling amplitude. Qualitatively, both VMC and VPI reveal the same phenomenon, except that the VMC data lie lower than the VPI data for the same k values. The reason is due to the difference between the VMC and VPI OD as observed in Fig. 1. If one inspects the latter figure closely, one can see that the VMC peaks are slightly narrower than the VPI peaks. The VMC peaks at the edges have a higher amplitude than the VPI peaks, but the central peaks almost match each other. In any case, we are using the overlap integral to provide a qualitative measure only. One can see again the dependence of the VMC method on the trial wave function used, as mentioned in subsection II L above.

Figure 4 is as in Fig. 3; but it shows the VMC case for $N = 40$ and $V_0 = 20$ for k values of π and 1.2π (solid circles and triangles, respectively). For $k = 1.2\pi$, I_{overlap} decreases overall with increasing a_c, whereas for $k = 1.0\pi$ it rises somewhat up to $a_c = 0.18$ and then begins to drop. However, the response is still weak and insignificant. Hence, a slightly stronger response is obtained for the tunneling amplitude when using a larger N. Further, the effect of changing $d = \pi/k$ on I_{overlap} is much more pronounced than changing a_c. Signals for a stronger response of our systems to the rise of a_c are found in the single-particle properties such as the width of the single-particle wave function and the onsite interaction energy.

In order to provide a measure for the single-particle tunneling amplitude, we evaluate $\langle J\rangle$ [Eq. (16)] between two chosen lattice sites: the center (000) and a first nearest neighbor $(00-1)$. Further, the onsite repulsive interaction energy $\langle U_{(000)}\rangle$ is obtained from Eq. (18) and used to calculate the ratio J/U (where $J \equiv \langle J_{(000)\to(00-1)}\rangle$ and $U \equiv \langle U_{(000)}\rangle$) to determine whether the current systems are SF or MI. The critical value for a SF-MI transition is $zJ/U = 0.172$ [1] below which one enters the MI regime.

Figure 5 displays $\langle J_{(000)\to(00-1)}\rangle$ versus a_c for the same systems as in Fig. 3. $\langle J_{(000)\to(00-1)}\rangle$ decreases with a_c for $k > 1.0\pi$ and remains almost constant for $k = 1.0\pi$. Hence, single-particle tunneling is gradually suppressed as the repulsion between the bosons rises for $k > 1.0\pi$.

Figure 6 displays $\langle J_{(000)\to(00-1)}\rangle/\langle U_{(000)}\rangle$ versus a_c for essentially the same systems as in Fig. 3 and various k: VMC at $k = 1.2\pi$ (solid triangles), VPI at $k = 1.2\pi$ (open triangles),

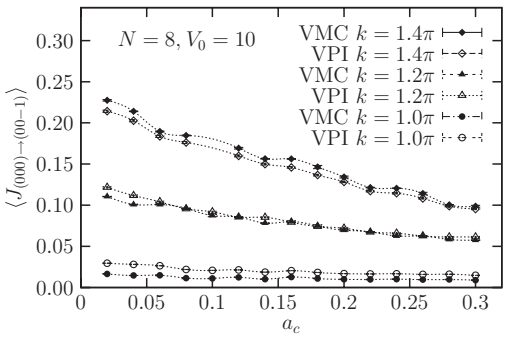

FIG. 5. Single-particle tunneling amplitude J [Eq. (16)] versus the HS diameter a_c between two lattice sites (000) and $(00-1)$ for the same systems of Fig. 3 at the indicated values of k: VMC and VPI results at $k = 1.4\pi$ (solid and open diamonds, respectively); similarly at $k = 1.2\pi$ (solid and open triangles); $k = 1.0\pi$ (solid and open circles). The dotted lines are a guide to the eye. The V_0 and $\langle J_{(000)\to(00-1)}\rangle$ are in units of $\hbar\omega_{\text{ho}}$, k is in units of a_{ho}^{-1}, and a_c is in units of a_{ho}.

VMC at $k = 1.0\pi$ (solid circles), and VPI at $k = 1.0\pi$ (open circles). One can see that zJ/U lies way above the critical value 0.172 which places our systems in the SF regime.

B. Width of the single-particle wave function in each potential well

As already indicated under Sec. II, the width of the single-particle wave function $\phi(\mathbf{r},\mathbf{R}_n)$ [Eq. (6)] in each well is expected to decrease with a rise of the HS repulsion in order to counteract the effects of a broadening due to the Jastrow function for a larger number of particles than $N = 8$. The width, or, better, the inverse of it, is described by the VMC parameter β in Eq. (6). In Fig. 7, the VMC parameter β of $\phi(\mathbf{r},\mathbf{R}_n)$, is displayed as a function of a_c. The open triangles display β for the HS Bose gas of Fig. 3 at $k = 1.2\pi$; solid circles: HS Bose gas of Fig. 4 at $k = \pi$. It is found that this width ($\propto 1/\sqrt{\beta}$) decreases with the rise in the repulsion for $N = 40$ and remains almost constant for $N = 8$.

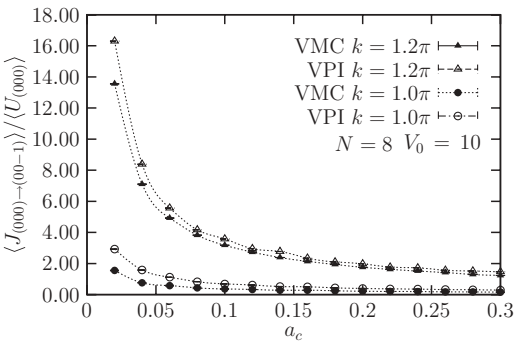

FIG. 6. Ratio of the tunneling amplitude and onsite repulsive energy $\langle J_{(000)\to(00-1)}\rangle/\langle U_{(000)}\rangle$ as a function of the HS diameter a_c for the same systems of Fig. 3 at the indicated values of k: VMC and VPI results at $k = 1.2\pi$ (solid and open triangles); similarly for $k = 1.0\pi$ (solid and open circles). The V_0, $\langle J_{(000)\to(00-1)}\rangle$ and $\langle U_{(000)}\rangle$ are in units of $\hbar\omega_{\text{ho}}$, k is in units of a_{ho}^{-1}, and a_c is in units of a_{ho}.

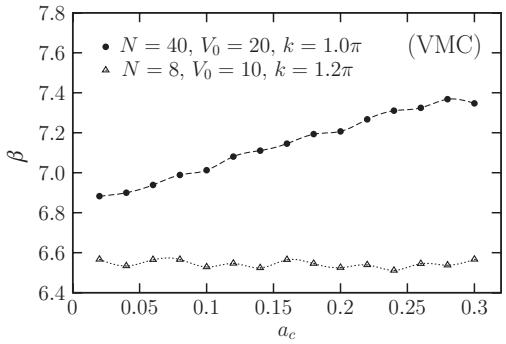

FIG. 7. VMC parameter β of the trial wave function [Eq. (6)] as a function of the hard-sphere diameter a_c for two HS Bose gas systems in a CHOCL of $3 \times 3 \times 3$ sites. Open triangles: HS Bose gas of Fig. 3 at $k = 1.2\pi$. Solid circles: HS Bose gas of Fig. 4 at $k = \pi$. The dashed and dotted lines are a guide to the eye. The a_c is in units of $a_{\rm ho}$, k is in units of $a_{\rm ho}^{-1}$, V_0 is in units of $\hbar\omega_{\rm ho}$, and β is in units of $a_{\rm ho}^{-2}$.

C. Onsite interaction energies

The chief goal of this subsection is to show that the onsite repulsive energy $\langle U_n \rangle$ at the lattice sites n rises with increasing HS diameter a_c, although the corresponding occupancy of a lattice site n may be dropping. Further, another goal is to reveal a symmetric distribution of the total repulsive potential energy around the trap center. This is a proof that VMC as well as VPI describes the systems correctly.

Discrete distributions of $\langle U_n \rangle$ over all 27 lattice sites, for systems of $N = 8$, $V_0 = 10$, $k = \pi$, and two cases $a_c = 0.02$ and 0.10, are displayed in Figs. 8 and 9, respectively. The abscissa display the site index n. All $\langle U_n \rangle$ which have the same magnitude within a small margin of error belong to the same set of nearest neighbors from the central lattice site. That is, moving vertically from the tip of the discrete distribution down to the bottom, we move from the center to the first, second, and third set of nearest neighbors, respectively. The distribution is uniform around the trap center. The effects of the external trap are manifested in the magnitude of $\langle U_n \rangle$ which is highest at the center and declines toward the edges of the trap due to the factor $\exp(-4\alpha r^2)$ in Eq. (18). Obviously, a large percentage of the particles is concentrated at the central lattice site. It is anticipated, then, that if the strength

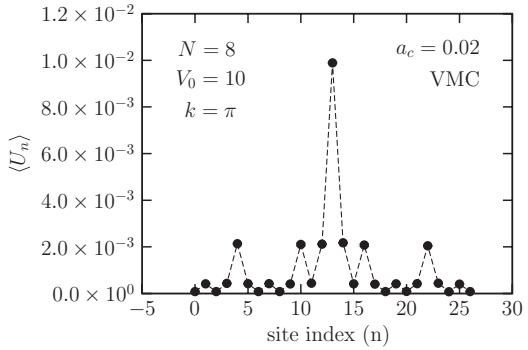

FIG. 8. Average VMC onsite repulsive interaction energy $\langle U_n \rangle$, at each lattice site n, for the HS Bose gas of Fig. 3 at $a_c = 0.02$ and $k = \pi$. The $\langle U_n \rangle$ and V_0 are in units of $\hbar\omega_{\rm ho}$; k is in units of $a_{\rm ho}^{-1}$.

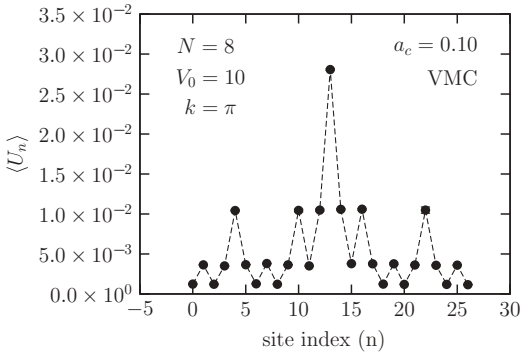

FIG. 9. As in Fig. 8; but for $a_c = 0.10$. The $\langle U_n \rangle$ and V_0 are in units of $\hbar\omega_{\rm ho}$; k is in units of $a_{\rm ho}^{-1}$.

of the external harmonic trap is increased further, this causes a drop in the density $\sim \exp(-2\alpha r^2)\,|\phi(\mathbf{r}, \mathbf{R}_n)|^2$ (and hence $\langle U_n \rangle$) at the lattice sites toward the edges of the trap and a certain rise at the center of the trap. Continuing the rise of this strength will force all the bosons to eventually occupy the central lattice site, and only if their HS diameter is of a magnitude that allows all of them to fit inside one lattice-site volume $\sim 4\pi(d/2)^3/3$. Thus, a large amount of repulsive potential energy would be stored in the trap center. The patterns of Figs. 8 and 9 show also that the bosons minimize their potential energy arising from the external harmonic trap by maximizing their occupancy of the trap center and minimizing it toward the edges of the trap. In the discussion section, we show later that the external HO trap plays a chief role in preventing the wave functions from largely broadening.

Next, the goal is to show that a linear increase in the interaction parameter g overwhelms a decrease in the occupancy $\langle N_{(pqr)} \rangle$ with the net effect that $\langle U_{(pqr)} \rangle$ rises. First, $\langle U_n \rangle$ is displayed as a function of a_c in Figs. 10 and 11 for the systems of Fig. 3 at $k = \pi$ and 1.2π, respectively, and for four lattice sites: $\mathbf{R}_n \equiv (000)$ [VMC (solid) and VPI (open circles)], $(00-1)$ (as before but with up triangles), (011) (then diamonds), and (111) (finally with down triangles), representative of the whole lattice. In general, $\langle U_{(pqr)} \rangle$ rises with a_c signaling a rise in the repulsive energy of the particles

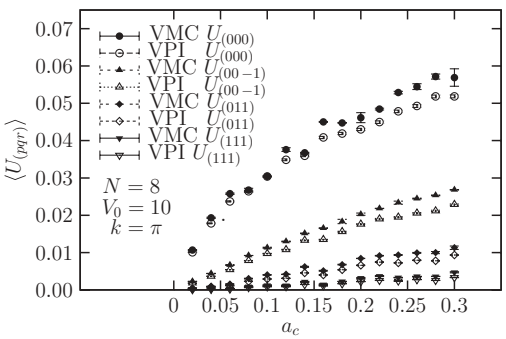

FIG. 10. Average onsite repulsive interaction energy $\langle U_{(pqr)} \rangle$ vs. the hard-sphere (HS) diameter a_c at four lattice sites representative of the whole lattice. The system is the HS Bose gas mentioned in Fig. 3 at $k = \pi$. Solid and open circles: VMC and VPI results for $\langle U_{(000)} \rangle$. Solid and open up triangles: likewise for $(00-1)$. Solid and open diamonds: for (011). Solid and open down triangles: for (111). The a_c is in units of $a_{\rm ho}$, k is in units of $a_{\rm ho}^{-1}$, and V_0 is in units of $\hbar\omega_{\rm ho}$.

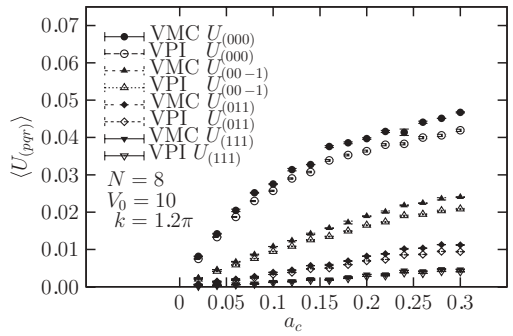

FIG. 11. As in Fig. 10; but for $k = 1.2\pi$. The $\langle U_{(pqr)} \rangle$ and V_0 are in units of $\hbar\omega_{\rm ho}$, a_c is in units of $a_{\rm ho}$, and k is in units of $a_{\rm ho}^{-1}$.

in each well. The rate of growth of $\langle U_{(pqr)} \rangle$ is largest for the trap center and declines toward the edges of the trap. Now Fig. 12 displays $\tilde{U}_{(pqr)} = \langle U_{(pqr)} \rangle / (4\pi a_c)$ for the same systems of Fig. 10 with the same labels used. That is $\tilde{U}_{(pqr)}$ is Eq. (18) divided by g, leaving us with an integral essentially similar to Eq. (20). One can see that $\tilde{U}_{(000)}$ decreases with increasing a_c, thus indicating indirectly a decline in the occupancy of the trap center. By closely inspecting the rest of the (pqr), $\tilde{U}_{(00-1)}$ remains almost constant with changing a_c, and a slight initial rise is observed for $\tilde{U}_{(011)}$ and $\tilde{U}_{(111)}$. Thus, for the trap center, a rise in a_c overwhelms a decline in $\tilde{U}_{(pqr)}$ given by Eq. (18), in other words, a drop in an indirect measure for the occupancy. Further, one notes that $\langle U_{(000)} \rangle$ at $a_c = 0.3, k = 1.2\pi$ is smaller than at $a_c = 0.3$, $k = 1.0\pi$, because there are fewer particles at $k = 1.2\pi$ than $k = 1.0\pi$. This can be seen in Fig. 16 below for the same latter systems.

D. Boson-optical lattice overlap

In this subsection, we evaluate $\langle I_{\rm boson-OL} \rangle$ [Eq. (17)] which measures the overlap of all the single-particle densities in the wells with the periodic optical lattice potential. In essence, it measures also the *total* tunneling amplitude of the particles into the optical lattice potential barriers. Figs. 13 and 14 display $\langle I_{\rm boson-OL} \rangle$ vs. a_c for the systems of Figs. 3 and 4, respectively and using the same labels. One can see that $\langle I_{\rm boson-OL} \rangle$ is practically invariant for $N = 8$, but the system with $N = 40$ reveals a slightly stronger response to changes in a_c. For example for $N = 8$ and $k = \pi$, the change in $\langle I_{\rm boson-OL} \rangle$

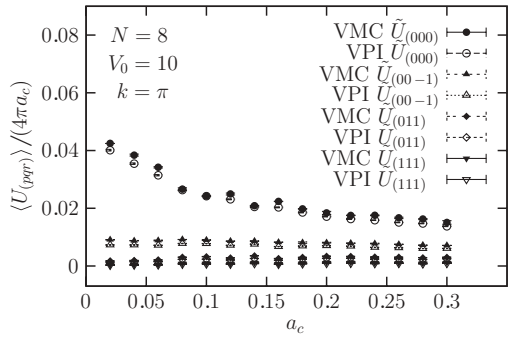

FIG. 12. As in Fig. 10; but for $\langle U_{(pqr)} \rangle / (4\pi a_c)$ versus a_c. Here $\tilde{U}_{(pqr)} = \langle U_{(pqr)} \rangle / (4\pi a_c)$. The $\langle U_{(pqr)} \rangle$ and V_0 are in units of $\hbar\omega_{\rm ho}$, and a_c is in units of $a_{\rm ho}$.

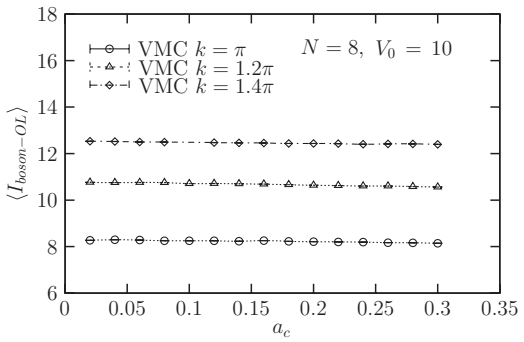

FIG. 13. VMC Boson-OL overlap integral [Eq. (17)] vs the hard-sphere diameter a_c for the systems of Fig. 3. The a_c is in units of $a_{\rm ho}$, k is in units of $a_{\rm ho}^{-1}$, and V_0 and $\langle I_{\rm boson-OL} \rangle$ are in units of $\hbar\omega_{\rm ho}$.

from $a_c = 0.02$ to 0.3 is only by -1.45%. The other changes for $N = 8$ are of the same order of magnitude. This in turn indicates, that the width of the wave functions in each well for these systems is practically invariant with the rise in repulsion. This may come as a surprise, since it is known [23,24] that at very large HS diameters such as the ones used here, the wave function ought to become very broad indeed. It seems that the localization effect of the optical lattice potential overwhelms the repulsive forces tending to broaden the wave function in each well. One further observes that $\langle I_{\rm boson-OL} \rangle$ increases with k in agreement with the results of Figs. 3 and 4, where $I_{\rm overlap}$ rises with increasing k.

Further, we note that in Fig. 14, $\langle I_{\rm boson-OL} \rangle$ rises notably with a_c indicating a rise in the total tunneling amplitude into the optical potential barriers. We were unable to obtain values of $\langle I_{\rm boson-OL} \rangle$ for $k = 1.2\pi$ beyond $a_c = 0.18$ as we could not find VMC energy minima for these systems. We must emphasize that the overlap of the bosons with the optical lattice potential is a different measure than $I_{\rm overlap}$, which measures the overlap of two wave functions in neighboring wells. Further, note that since in Fig. 4 $I_{\rm overlap}$ decreases with increasing a_c for $k = 1.2\pi$, the rise of $\langle I_{\rm boson-OL} \rangle$ indicates that the tunneling amplitude between neighboring wells away from the center of the trap may be rising with increasing a_c, because $\langle I_{\rm boson-OL} \rangle$ is a sum over all the single-particle densities overlapping with $V_{\rm opt}(\mathbf{r})$.

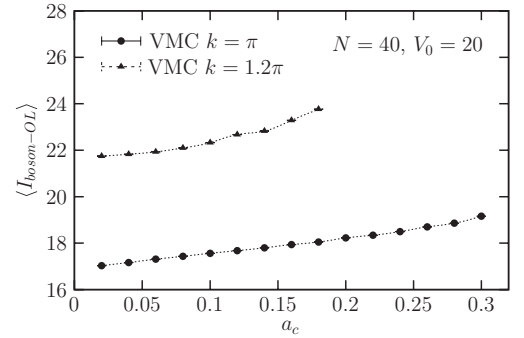

FIG. 14. As in Fig. 13; but for the systems of Fig. 4. The a_c is in units of $a_{\rm ho}$, k is in units of $a_{\rm ho}^{-1}$, and V_0 and $\langle I_{\rm boson-OL} \rangle$ are in units of $\hbar\omega_{\rm ho}$.

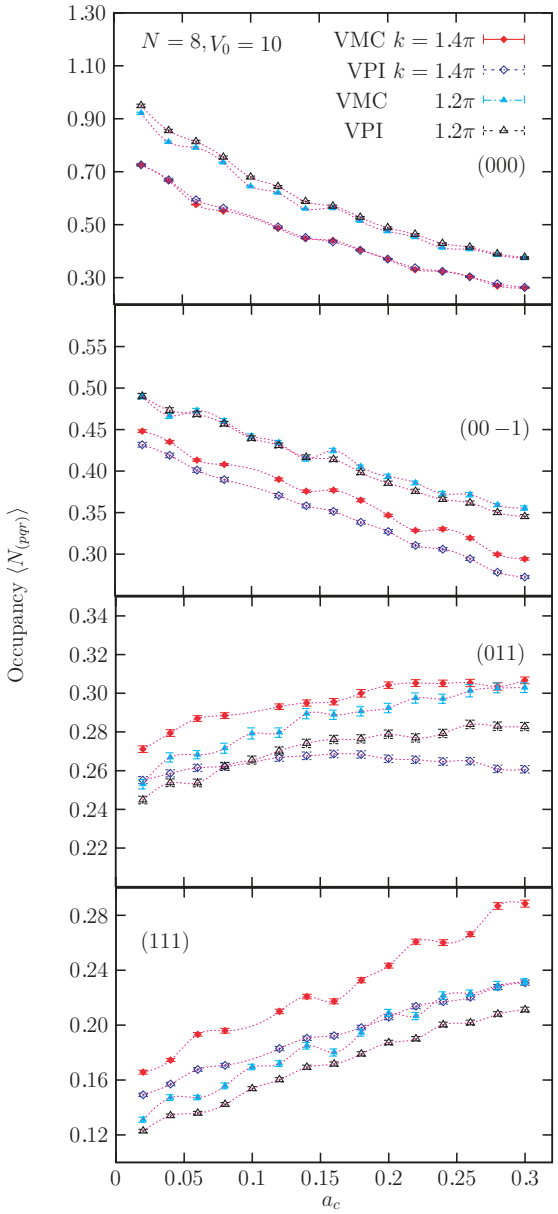

FIG. 15. (Color online) Average occupancy $\langle N_{(pqr)} \rangle$ vs. the hard-sphere diameter a_c at the four lattice sites (pqr) indicated, which are representative of the whole optical lattice. The system is the HS Bose gas of Fig. 3. Solid and open diamonds: VMC and VPI results for $k = 1.4\pi$, respectively. Solid and open triangles: likewise but for $k = 1.2\pi$. From top to bottom frame: $\mathbf{R}_{13} \equiv (000)$ is the center, $\mathbf{R}_{12} \equiv (00-1)$ the first, $\mathbf{R}_{17} \equiv (011)$ the second, and $\mathbf{R}_{26} \equiv (111)$ the third nearest neighbor to the center, respectively. Site indices n are according to Fig. 8. The a_c is in units of $a_{\rm ho}$, k is in units of $a_{\rm ho}^{-1}$, and V_0 is in units of $\hbar\omega_{\rm ho}$.

E. Occupancy of lattice sites

Figure 15 displays the average occupancy of four lattice sites $\langle N_{(pqr)} \rangle$ for systems of Fig. 3: $(pqr) \equiv (000)$, $(00-1)$, (011), and (111). Each frame is labeled by the corresponding lattice site. The solid and open diamonds display VMC and VPI results for $k = 1.4\pi$, whereas the solid and open triangles display them for $k = 1.2\pi$, respectively. The VMC results have been obtained by Eq. (20), whereas the VPI results from simple counting of the bosons in cubic bins. In frames (000) and $(00-1)$, the occupancy decreases with a_c, whereas in frames (011) and (111) it rises. The VMC and VPI results almost match for (000) and $(00-1)$ and are close to each other for (011) and (111). There is good agreement between the occupancies calculated by Eq. (20) and those obtained by counting. This indicates that the single-particle wave function in Eq. (6) is suitable to describe the bosons at each lattice site.

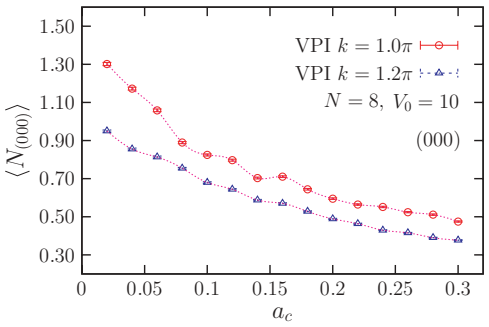

FIG. 16. (Color online) As in Fig. 15 but for $\langle N_{(000)} \rangle$ at $k = 1.0\pi$ compared with $k = 1.2\pi$. a_c is in units of $a_{\rm ho}$, k is in units of $a_{\rm ho}^{-1}$, and V_0 is in units of $\hbar\omega_{\rm ho}$.

Figure 16 displays $\langle N_{(pqr)} \rangle$ as in Fig. 15 but for VPI $\langle N_{(000)} \rangle$ at $k = 1.0\pi$ compared with $k = 1.2\pi$. Again, $\langle N_{(pqr)} \rangle$ decreases with increasing a_c.

F. Correlations

The VPI pair correlation function $g(r)$ for the systems of $N = 8$, $V_0 = 10$, $k = \pi$, and various a_c in the range $0.02 \leqslant a_c \leqslant 0.30$ are displayed in Fig. 17. It is observed that the correlations are strongest for $a_c = 0.02$ (crosses) and gradually weaken as a_c is increased up to 0.3 (triangles). The peak in $g(r)$ is largest for smallest a_c as the particles are able to cluster around each other in the deepest part of the well when a_c is small [52]. When a_c rises, they are driven to larger r values. This is because the Jastrow function, which determines the smallest distance the bosons are allowed to approach each other, starts from zero at a larger r as a_c rises thus increasing the closest distance of approach. Further, $g(r)$ is like a "spring" whose maximum compression is determined by a_c.

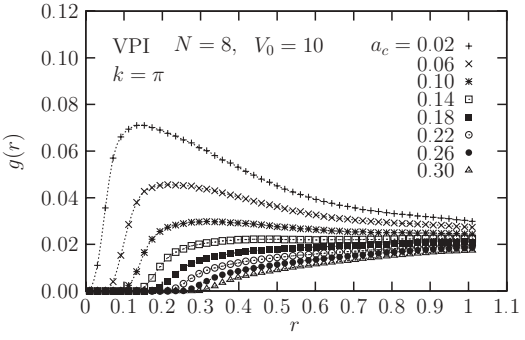

FIG. 17. VPI pair correlation function $g(r)$ for the indicated a_c. The system is the HS Bose gas of Fig. 3 at $k = \pi$. The r and a_c are in units of $a_{\rm ho}$, k is in units of $a_{\rm ho}^{-1}$, and V_0 is in units of $\hbar\omega_{\rm ho}$. $g(r)$ is in units of $a_{\rm ho}^{-3}$.

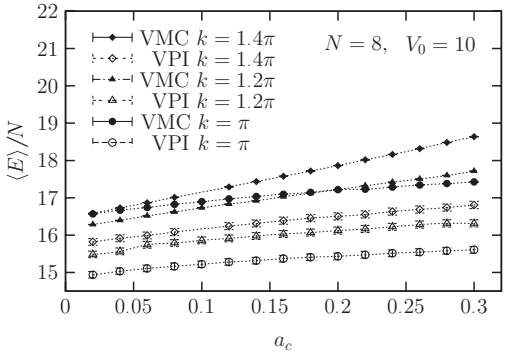

FIG. 18. Average energy per particle $\langle E \rangle / N$ vs. a_c for the HS Bose gas systems of Fig. 3 at the indicated values of k. Solid and open diamonds: VMC and VPI results for $k = 1.4\pi$. Solid and open triangles: likewise, but for $k = 1.2\pi$, and solid and open circles: $k = \pi$. The $\langle E \rangle$ and V_0 are in units of $\hbar\omega_{\rm ho}$, k is in units of $a_{\rm ho}^{-1}$, and a_c is in units of $a_{\rm ho}$.

G. Energy

The average Monte Carlo (MC) energies per particle $\langle E \rangle / N$ as functions of a_c for the systems of Figs. 3 and 4, are displayed in Figs. 18 and 19, respectively. Additionally, the energies for a system of $N = 2$ and $V_0 = 2$ are displayed in Fig. 20 as well. The same labels are used as in Fig. 5. [Solid (open) diamonds: VMC (VPI) results for $k = 1.4\pi$; triangles (as before): $k = 1.2\pi$; and circles: π, respectively.] We note that, for most of the systems considered, $\langle E \rangle / N$ changes almost linearly within the given range of a_c and at a much slower rate than HS Bose gases in pure harmonic traps [23,24]. For example, for $N = 2$ with $k = \pi$, the VPI $\langle E \rangle / N$ rises only by $\Delta E_{VPI}/N \sim +2.98\%$ from $a_c = 0.02$ to $a_c = 0.3$, despite the fact that there is a very large change in a_c (by a factor of 14!). Similarly for $N = 8$ and $k = \pi$, $\Delta E_{VPI}/N$ is $\sim +4.48\%$. However, $\Delta E_{VPI}/N$ for $k = 1.4\pi$ is more pronounced, being $\sim +6.26\%$. The corresponding VMC results are as follows: for $N = 2$ with $k = \pi$, $\Delta E_{VMC}/N \sim +4.48\%$, for $N = 8$ with $k = \pi$, $\Delta E_{VMC}/N \sim +5.20\%$, and for $N = 8$ with $k = 1.4\pi$, $\Delta E_{VMC}/N \sim +12.37\%$, respectively. For $N = 40$, $\Delta E/N$ changes at a much faster rate than for a lower N. Further, the energy $\langle E_{VMC} \rangle / N$ rises with increasing k.

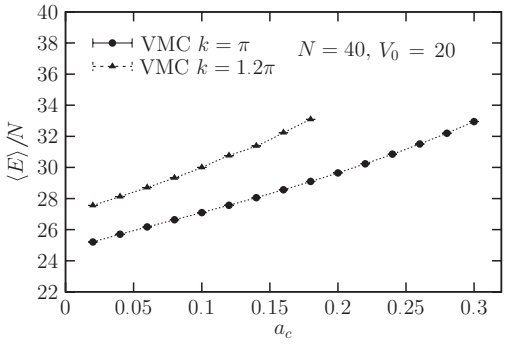

FIG. 19. As in Fig. 18 but for the HS Bose gases of Fig. 4. The $\langle E \rangle$ and V_0 are in units of $\hbar\omega_{\rm ho}$, k is in units of $a_{\rm ho}^{-1}$, and a_c is in units of $a_{\rm ho}$.

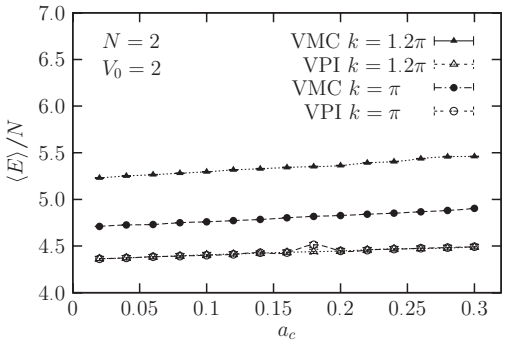

FIG. 20. As in Fig. 18 but for $N = 2$, $V_0 = 2$. a_c is in units of $a_{\rm ho}$. The $\langle E \rangle$ and V_0 are in units of $\hbar\omega_{\rm ho}$.

H. Optical density

In this section, the integrated VPI OD $\langle n_{2D}(x,y) \rangle$ for the previous systems is displayed at different a_c. The goal is to explore the effects of variations in the interactions on the OD profiles and on the tunneling amplitude. Particularly we show visually that, for a small number of particles, the width of the wave function in each well does not broaden with an increase in a_c, even up to order 0.1, and that practically the overlap between the wave functions does not change either.

Figure 21 displays the integrated VPI OD for $N = 2$, $V_0 = 2$, and $k = \pi$. From the top to bottom frames, $a_c = 0.02$, 0.14, and 0.30, respectively. As expected, the amplitude of the density is maximal at the center of the trap and lowest for the lattice sites near the edges of the trap. Further, the tunneling of the system into the potential barrier of the external harmonic trap is suppressed due to the steep rise of this barrier as one goes away from the center of the trap. Since the optical-lattice barrier height is very shallow, the wave function of the system is spread over the whole lattice, indicating the dominance of the tunneling process [1] over the localization effects of the optical lattice potential wells.

Figure 22 displays 1D density slices of Fig. 21 along the x axis and, additionally, three functions of the form (11) fitted to this density profile as in Fig. 2 previously. The fits reveal the extent of the overlap between the wave functions in neighboring wells. It is observed that this overlap does not change with a rise in a_c. The left and right fits are much broader than the central function and all three fitting functions have almost the same amplitude. In fact, the overlap here is between three wave functions as the left and right fits are able to spread over several trap lengths.

Figure 23 is the same as Fig. 21 but for $N = 8$ and $V_0 = 10$. Here, the bosons are more localized at the lattice sites, and the tunneling process is less dominant than the localization effects of the optical lattice. Again, the effects of the external trap are manifested: the density diminishes toward the edges of the trap. Figure 24 displays again the 1D slices of Fig. 23 along the x axis as in Fig. 22. Here, the overlap is much less pronounced than in Fig. 22, and the amplitude of the central peak is larger than the peaks at the edges. The left and right peaks do not overlap as in Fig. 22. It seems that a slight increase in the number of particles has a profound effect on the density profiles in that it changes the ratio of the amplitude of the central density to that of the density at the

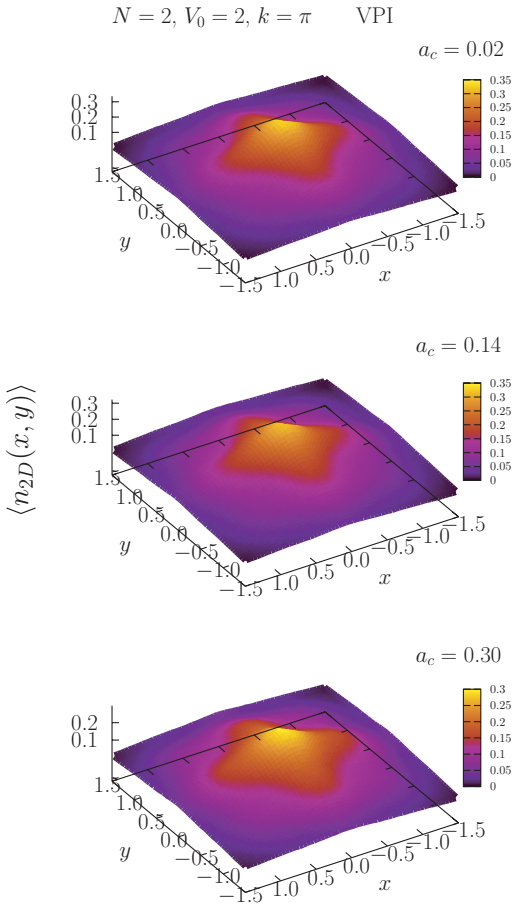

FIG. 21. (Color online) Integrated VPI OD for the HS Bose gas system of $N = 2$, $V_0 = 2$, and $k = \pi$, at three values of a_c in a CHOCL of $3 \times 3 \times 3$ lattice sites. From top to bottom frames: $a_c = 0.02$, 0.14, and 0.30, respectively. The x, y, and a_c are in units of $a_{\rm ho}$ and V_0 is in units of $\hbar\omega_{\rm ho}$. $\langle n_{2D}(x,y)\rangle$ is in units of $a_{\rm ho}^{-2}$.

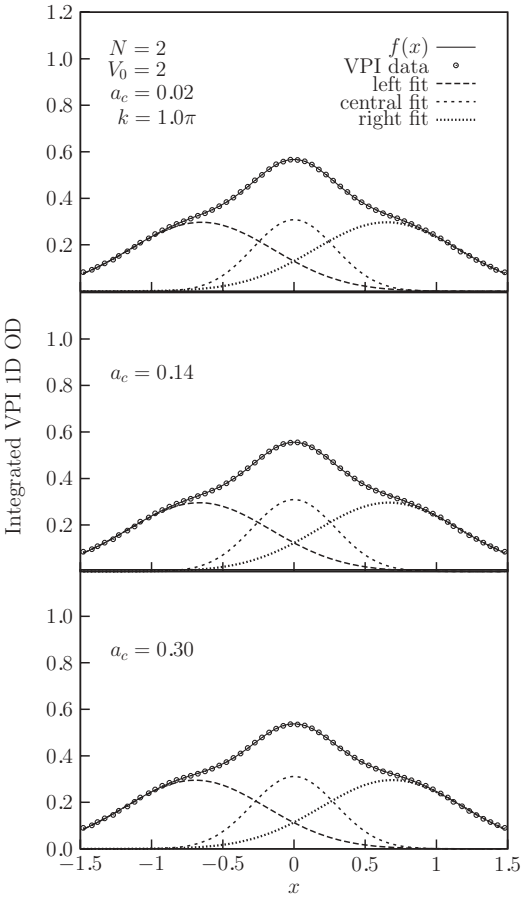

FIG. 22. Integrated one-dimensional (1D) OD slices $n_{1D}(x)$ of Fig. 21 along the x axis. The same legends are used as in Fig. 2, except for VPI data. The x and a_c are in units of $a_{\rm ho}$, k is in units of $a_{\rm ho}^{-1}$, and V_0 is in units of $\hbar\omega_{\rm ho}$. The VPI 1D OD is in units of $a_{\rm ho}^{-1}$.

trap edges. Further, the width of the densities at the edges of the trap for $N = 8$ has dropped by almost 2 trap lengths as compared to the case for $N = 2$. Nevertheless, there is still overlap between the wave functions in the neighboring wells even at high repulsion. For $N = 8$, the amplitude of the central peak declines with increasing a_c. The change in the height of the central peak as one increases a_c from 0.02 to 0.14 is $\sim$33.3%. Remarkably, even with strongly repulsive bosons, the density of the system in each well largely peaks at the potential minimum of each well instead of being broader and more evenly distributed around each lattice site as in Fig. 21.

The latter situation does not change very much for a larger number of particles. Figure 25 displays the integrated VMC OD for the system of $N = 40$, $V_0 = 20$, and $k = 1.2\pi$ and Fig. 26 its density slices, as in the latter figures for the OD. Again, the peaks in each well do not broaden very much with a rise in a_c. The central peak loses amplitude in favor of a rise in the amplitude of the peaks at the edges. On closely inspecting the area of the overlap between neighboring peaks, one can depict a small decline in the tunneling amplitude of the system as a_c is increased. In Figs. 24 and 26, the positions of the left and right peak maxima shift slightly to the left and right, respectively, as a_c is increased.

IV. EFFECT OF OPTICAL-LATTICE BARRIER HEIGHT ON TUNNELING

Although our chief goal was to fix V_0 and vary a_c only, we nevertheless divert a little and explore the evolution of a HS Bose gas in a CHOCL by changing V_0 and fixing a_c. The goal is to compare between the roles of V_0 and a_c (previously) in determining the overlap between wave functions in neighboring wells in the presence of an external harmonic trap.

Figure 27 displays the evolution of the integrated OD with changing V_0 (map view) for a system of $N = 8$ particles, $k = \pi$, and fixed HS diameter $a_c = 0.14$. From top to bottom: $V_0 = 1$, 2, 6, and 10, respectively. As V_0 is increased, the overlap of the wave functions in neighboring wells drops substantially and the change is *gradual*. Figure 28 displays, similarly to Figs. 22 and 24, again the density slices of Fig. 27 along the x axis, where one can clearly see how the overlap, and therefore the tunneling amplitude, drops. We anticipate then, that as V_0 is increased further, the tunneling will drop substantially, and may even lead to a MI state. Note, however, that the amplitude

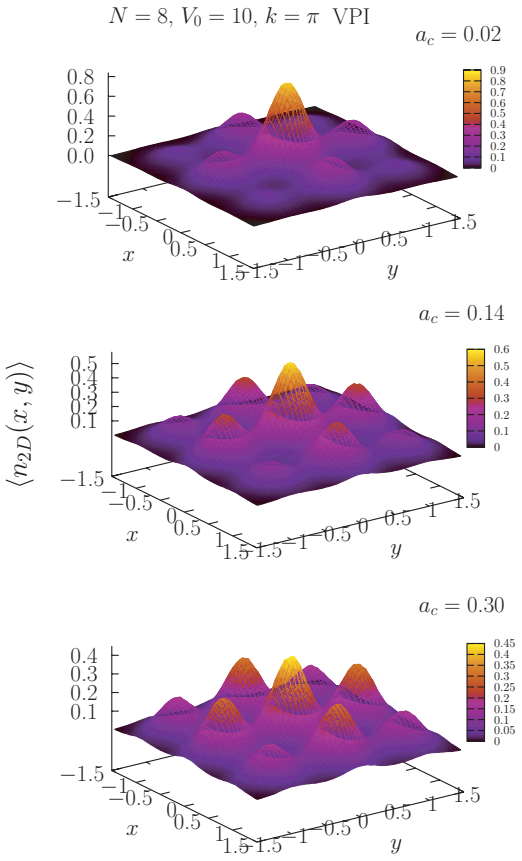

FIG. 23. (Color online) As in Fig. 21 but for $N = 8$ and $V_0 = 10$. The x, y, and a_c are in units of $a_{\rm ho}$ and V_0 is in units of $\hbar\omega_{\rm ho}$. $\langle n_{2D}(x,y)\rangle$ is in units of $a_{\rm ho}^{-2}$.

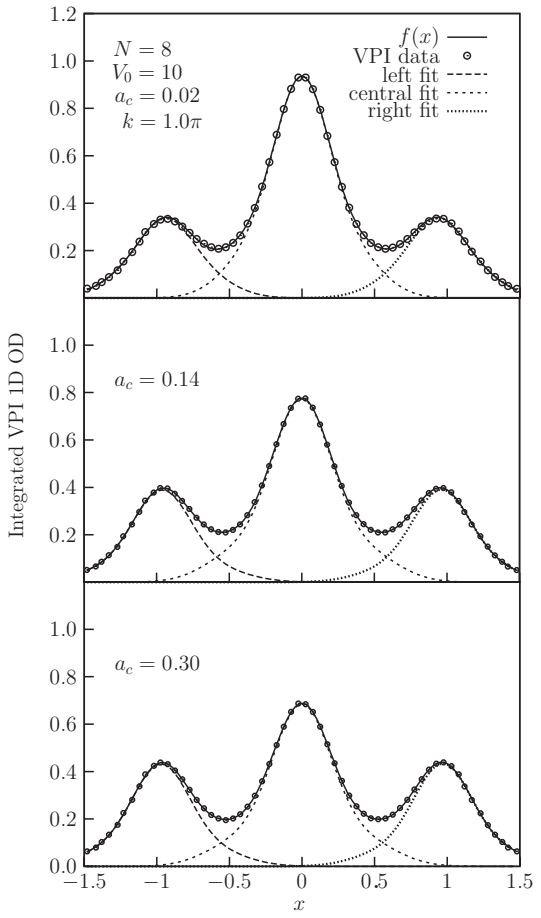

FIG. 24. As in Fig. 22 but for $N = 8$ and $V_0 = 10$. The x and a_c are in units of $a_{\rm ho}$, k is in units of $a_{\rm ho}^{-1}$ and V_0 in units of $\hbar\omega_{\rm ho}$. The VPI 1D OD is in units of $a_{\rm ho}^{-1}$.

of the central peak rises with increasing V_0. Compared to the previous figures, then, V_0 has a much more profound effect in changing the tunneling amplitude than a_c.

V. DISCUSSION AND CONCLUSION

In summary, we have investigated the effects of strongly repulsive interactions on the tunneling amplitude of HS bosons confined in a simple cubic optical lattice plus an external, tight, spherical harmonic trap. The tunneling amplitude was measured in two ways: (i) by the overlap integral of the wave functions in neighboring wells and (ii) by an exchange integral $\langle n|H|n+1\rangle$ between two neighboring wells n and $n+1$. The external harmonic trap was introduced in order to cause an inhomogeneiety in the density distribution of the trapped system.

It was found that for small N, the tunneling amplitude practically shows no change with increasing the boson-boson repulsion at fixed lattice spacing $d = \pi/k$. This is mainly because the width of each localized wave function does not broaden with a rise in the repulsive forces. The tunneling amplitude, however, rises by reduction of d at fixed a_c. Even at very large repulsion, tunneling is still present in the system and does not vanish completely. Further, the Wannier function used in our setup is sufficiently delocalized that it would seem most likely to describe a SF state. We prove this further in subsection V D below.

The energies change only weakly with increasing a_c for $N = 2$, but a more pronounced change is observed for $N = 8$ and is much larger for $N = 40$. The occupancy of the central and first nearest neighbor sites drops with increasing a_c, and rises at the second and third nearest-neighbor sites.

A. Occupancy and onsite interaction energies

Although the occupancy of particles in Fig. 15 at sites (000) and (00 −1) drops with increasing a_c causing a drop in the density at the central lattice site, the corresponding $\langle U_{(000)}\rangle$ and $\langle U_{(00-1)}\rangle$ still rise. Thus the effect of increasing g via a_c on $\langle U_{(pqr)}\rangle$ overwhelms that of the drop in the occupancy at each lattice site. The net result is that $\langle U_{(pqr)}\rangle$ increases with increasing g. Further, the occupancy of the lattice sites plays a crucial role in determining the relative magnitudes of $\langle U_{(pqr)}\rangle$. Since (000) for $k = 1.2\pi$ has the highest occupancy at all a_c, in Fig. 11 it has also the highest onsite repulsion. A similar conclusion can be made about Fig. 10 for $k = \pi$. Then with decreasing occupancy, the onsite repulsion decreases in the order $U_{(000)}$, $U_{(00-1)}$, $U_{(011)}$, and $U_{(111)}$ at all a_c. In Fig. 15, one can see also that for $k = 1.2\pi$ (111) has the lowest occupancy.

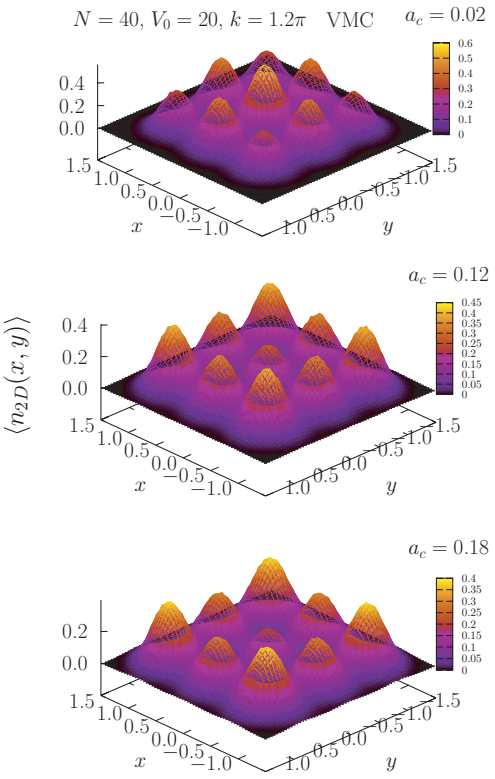

FIG. 25. (Color online) As in Fig. 21 but (using VMC) for $N = 40$, $V_0 = 20$, and $k = 1.2\pi$. The x, y, and a_c are in units of $a_{\rm ho}$ and V_0 is in units of $\hbar\omega_{\rm ho}$. $\langle n_{2D}(x,y)\rangle$ is in units of $a_{\rm ho}^{-2}$.

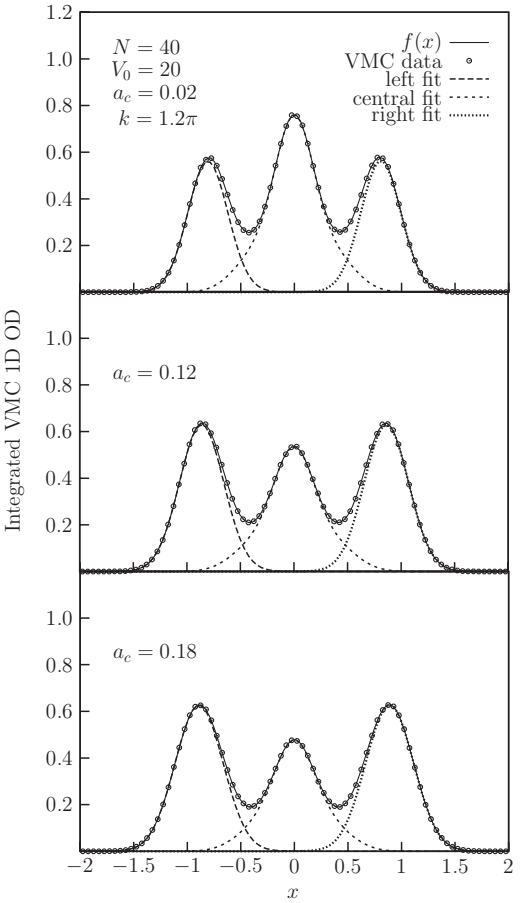

FIG. 26. As in Fig. 22 but (using VMC) for $N = 40$, $V_0 = 20$, and $k = 1.2\pi$. The x and a_c are in units of $a_{\rm ho}$, k is in units of $a_{\rm ho}^{-1}$ and V_0 in units of $\hbar\omega_{\rm ho}$. The VMC 1D OD is in units of $a_{\rm ho}^{-1}$.

In equilibrium, one could assume that there are as many particles tunneling into a lattice site as out which preserves the occupancy at each lattice site in equilibrium [52]. When a_c is changed, the particles relocate themselves in order to reach a new equilibrium configuration. If a_c is increased, particles are pushed out of the central site and occupy others until a new equilibrium configuration is reached again. Due to the external trap they are not able to tunnel further away from the edges of the trap. Further, note it is possible that during the equilibration process some particles, having tunneled from the center of the trap to the first neighbors, continue tunneling to the second and third. In fact, it would be interesting to know how the particles' motion is channelled along the sites of a larger simple cubic optical lattice, as the repulsion between the bosons is increased. Figure 15 displays noninteger occupancies of the lattice sites. We do not get integer occupancy because in MC one has only a probability of finding particles, particularly in the Wannier form of a single-particle wave function. Overall, then, the particles are fragmented [38].

B. Optical density and tunneling

As we have seen in Fig. 2 and Figs. 21–26, as much as the repulsion was increased, the overlap between neighboring wells did not change significantly, even at large N. But the change in the overlap is more pronounced if one increases V_0 while keeping a_c fixed. This was the situation displayed in Figs. 27 and 28. We conclude, then, that tunneling can be reduced more effectively by increasing V_0 than the HS repulsion between the bosons, a_c.

Similarly to our findings in subsection III H, Greiner *et al.* [1] showed, by applying the Bose-Hubbard (BH) model to a 3D optical lattice, that if the tunneling dominates the BH Hamiltonian, the single-particle wave functions are spread over the whole lattice, and phase coherence existing between the lattice sites forms a SF. On the other hand, if the atom-atom interactions dominate, the single-particle wave functions become localized at their lattice sites. Even in the highly repulsive regime, tunneling is still present.

In Fig. 27, if one keeps increasing V_0, we anticipate that the tunneling amplitude will drop much further.

C. The role of the lattice spacing $d = \pi/k$

In Figs. 3 and 4 the increase in k increases the tunneling amplitude. Increasing k causes the first nearest-neighbor lattice sites to approach the center of the trap due to a reduction in the lattice spacing $d = \pi/k$. The total volume of the external harmonic trap, however, does not change as the reader might think since the trapping frequency is kept fixed. As a result, the maximal heights of the potential barriers, resulting from the superposition of the optical lattice potential on an external harmonic potential, decline as the positions of the potential

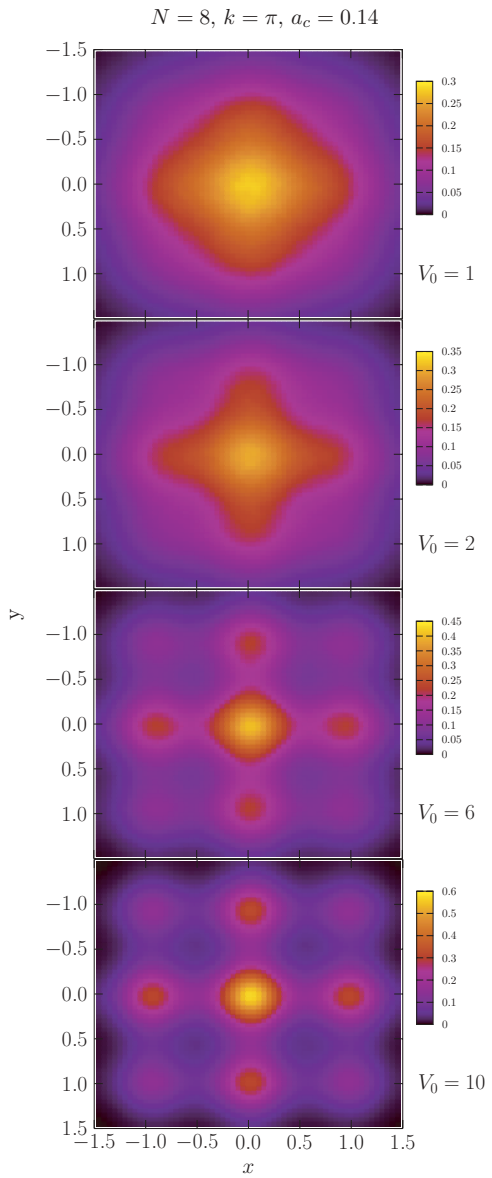

FIG. 27. (Color online) Map view of integrated VPI OD for various optical-lattice barrier heights V_0. The system is a HS Bose gas of $N = 8$, fixed $a_c = 0.14$, and $k = 1.0\pi$ which is confined in a CHOCL of $3 \times 3 \times 3$ lattice sites. From top to bottom: $V_0 = 1$, 2, 6, and 10 in units of $\hbar\omega_{\rm ho}$. The x, y, and a_c are in units of $a_{\rm ho}$ and k is in units of $a_{\rm ho}^{-1}$.

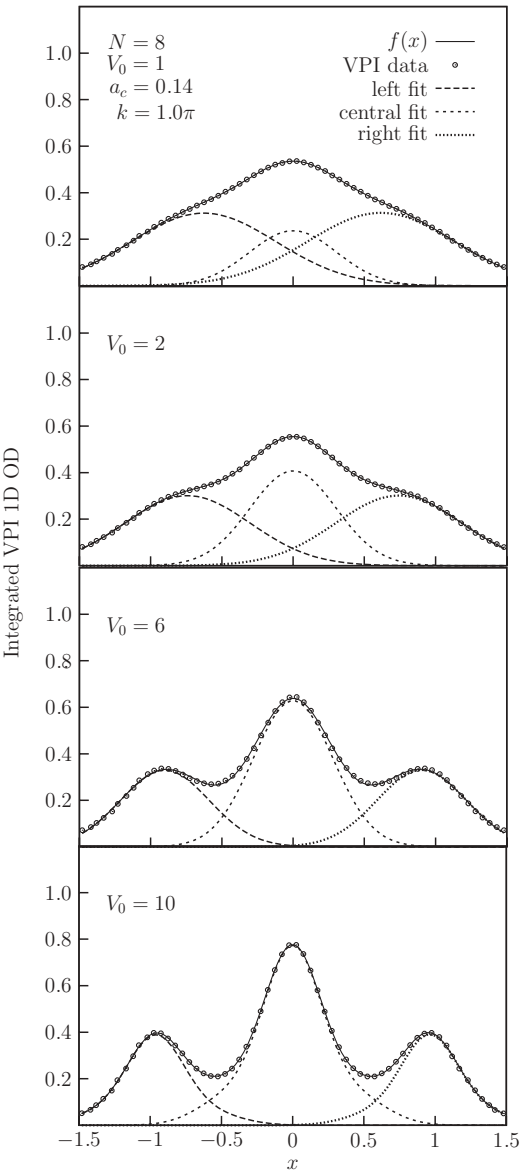

FIG. 28. Density slices of Fig. 27 along the x axis. The legends are as in Fig. 22. The x and a_c are in units of $a_{\rm ho}$, k is in units of $a_{\rm ho}^{-1}$, the VPI 1D OD is in units of $a_{\rm ho}^{-1}$, and V_0 is in units of $\hbar\omega_{\rm ho}$.

maxima approach the trap center. Consider hence the following argument in 1D. If r_0 is the distance of a potential maximum from the center of the trap, then its maximum height is

$$V(r_0) = V_0 \sin^2(kr_0) + \tfrac{1}{2}r_0^2, \tag{25}$$

where in this case $\sin(kr_0) = 1$. Hence, increasing k causes r_0 to decrease and thus $V(r_0)$. The latter fact allows a rise in the tunneling rate between two neighboring lattice sites. However, note that this scenario is specific to this type of potential which is a superposition including an external spherically symmetric harmonic trap. One may not observe this phenomenon if the external harmonic trap is absent.

D. The effects of the external harmonic trap

In order to demonstrate that the external HO trap indeed prevents the wave functions in each well from broadening with increasing a_c, we performed a numerical solution to the time-dependent GPE in 1D using the *NDSolve* utility in MATHEMATICA. The goal was to trace the evolution of the width of the wave function in each well. The time-dependent Gross-Pitaevskii equation (TDGPE) in units of the trap reads:

$$\frac{\mathbf{i}}{\omega_{\rm ho}}\frac{\partial\psi}{\partial t} = -\frac{1}{2}\frac{\partial^2}{\partial x^2}\psi + [V_{\rm ho}(x) + V_{\rm opt}(x)]\psi + g_{1D}|\psi|^2\psi, \tag{26}$$

where $\psi \equiv \psi(x,t)$, $V_{\rm ho}(x) = \frac{1}{2}x^2$, and $V_{\rm opt}(x) = V_0[\sin(kx)]^2$ are the HO and OL potentials in 1D, respectively, and $g_{1D} = 2a_c$ [51] is the 1D interaction parameter. Two

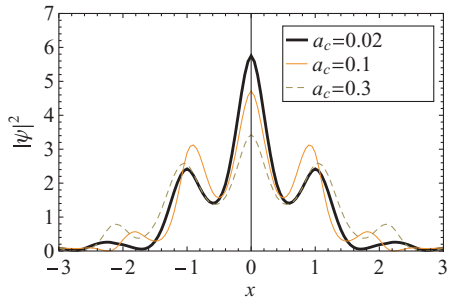

FIG. 29. (Color online) Densities $|\psi|^2$ of time-evolving 1D HS Bose gases in an optical lattice plus external harmonic trap at $\omega_{\rm ho}t = 10$ for different HS diameters. Here $V_0 = 10$ and $k = \pi$. Thick black line: $a_c = 0.02$; thin orange line: $a_c = 0.1$; dashed gray line: $a_c = 0.3$. The densities were obtained from a numerical solution of the time-dependent Gross-Pitaevskii equation (26) using MATHEMATICA. The x and a_c are in units of the trap, whereas $|\psi|^2$ is in units of $a_{\rm ho}^{-1}$.

cases are examined: the first is for different HS diameters a_c; the second is for two HO traps of different strength using the same a_c. Figure 29 displays the first case, where the density $|\psi(x,t)|^2$ at $\omega_{\rm ho}t = 10$ is shown for three a_c, ranging from the intermediate to the strongly interacting regime. The value of $\omega_{\rm ho}t$ was chosen arbitrarily larger than the time at which the TDGPE has evolved to the ground-state solution, beyond which it stopped changing with time. One can see that the wave functions in each well do not broaden significantly in the presence of an external HO trap. The two peaks, immediately next to the central one near $x \sim \pm 1$, shift somewhat away from the center of the trap as a_c is increased. In contrast to the three-dimensional densities of the present work, some more structure is revealed at the edges of the trap signified by small additional peaks around $x = \pm 2$. The wave functions obtained here from MATHEMATICA look remarkably similar to the ones generated from our trial wave function using VMC and VPI. A GPE, however, can only describe a BEC and therefore we conclude that our systems are SF even in the strongly interacting regime, basing on the similarities above. This strengthens our previous argument that perhaps our wave function most likely describes an SF. An MI state, on the other hand, cannot be described by a GPE. For the second case, Fig. 30 displays $|\psi(x,t|^2$ as in Fig. 29 but for $a_c = 0.1$ only and two traps: $V_{\rm ho}(x) = (1/2)x^2$ (solid black line) and

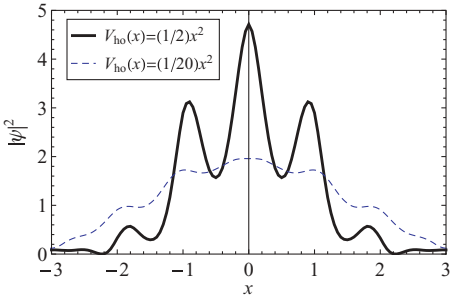

FIG. 30. (Color online) As in Fig. 29 but for $a_c = 0.1$ only and two different HO traps. Solid black line: $V_{\rm ho}(x) = \frac{1}{2}x^2$; dashed blue line: (weaker trap) $V_{\rm ho}(x) = \frac{1}{20}x^2$. The $V_{\rm ho}(x)$ is in units of $\hbar\omega_{\rm ho}$ and x is in units of $a_{\rm ho}$. $|\psi|^2$ is in units of $a_{\rm ho}^{-1}$.

$V_{\rm ho}(x) = (1/20)x^2$ (dashed blue line). For the latter trap, the wave functions in each well are broader than for the former stronger trap and the system begins to reach out to larger trap lengths. Hence, it looks like an external HO trap does indeed prevent our wave functions from broadening significantly in each well. If no external confinement were used, the bosons would be free to move everywhere within the optical lattice.

E. Energy

The rise of $\langle E\rangle/N$ with k in Figs. 18, 19, and 20 could be attributed to Heisenberg's uncertainty principle. A decline in the available volume the bosons can occupy in the optical lattice wells reduces the uncertainty in their positions. Thus, the uncertainty in their momenta increases and as a result their kinetic energy (quantum pressure) rises. Further, it is expected that the density of the bosons in each well rises as they get squeezed together by a reduction in d. It can also be seen that a change in k has a more profound effect on E than a change in a_c. Therefore, the lattice dimension seems to play a profound role in determining the SF properties of bosons in optical lattices in that it can substantially control the tunneling amplitude between neighboring wells.

F. Other work

Similarly to Bach and Rzążewski [53], we used Gaussians of the form $\exp[-\alpha(x - x_n)^2]$ but weighted by a polynomial as in Eq. (6). These authors determined that the mobility of the atoms, as described by the hopping parameter t and their interactions U, is controlled by the optical-lattice barrier height. If this barrier is shallow, the atoms become delocalized over the whole lattice as it almost occurs in Fig. 21.

Li *et al.* [6] investigated the SF to MI transitions in atomic BECs confined in optical lattices by using the BH model. Using an isotropic cubic lattice, they have chosen a variational trial function of the form $g(u) = (1 + \alpha u^2)\exp(-\beta u^2)$ (a Wannier function); our single-particle wave function is the same as theirs, except for an additional term $\propto u^4$ [Eq. (6)]. They addressed the possibility of observing SF to MI transitions for an average lattice-site occupancy larger than one. It was noted that by increasing the repulsion between the lattice bosons, their wave function in each well broadens, thus enhancing J between neighboring lattice sites. In contrast, our atomic clouds did not expand due to the presence of external confinement. Li *et al.* evaluated the on-site interaction energy by variationally minimizing the energy with respect to the parameters α and β.

Paredes [11] studied the dynamics of an ultracold interacting Bose gas confined in a 1D potential composed of a finite number of wells. His goal was to investigate Josephson tunneling and argued that only a finite number of wells is needed for this purpose. In essence, we are following a similar approach in that we use only 27 lattice sites but in 3D. Indeed, the investigation of tunneling in a finite number of wells could help us advance forward the design of Josephson tunneling junctions.

ACKNOWLEDGMENTS

Interesting and enlightening discussions with Saverio Moroni and William Mullin are gratefully acknowledged. We

thank William Mullin for a critical reading of the manuscript. One of the authors (A.R.S.), gratefully acknowledges the International Center for Theoretical Physics for providing computational access to their GRID cluster facility.

[1] M. Greiner, O. Mandel, T. Esslinger, J. W. Hänsch, and I. Bloch, Nature **415**, 39 (2002).
[2] J. A. M. Huhtamäki, M. Möttönen, J. Ankerhold, and S. M. M. Virtanen, Phys. Rev. A **76**, 033605 (2007).
[3] S. Fölling, S. Trotzky, P. Cheinet, M. Feld, R. Saers, A. Widera, T. Müller, and I. Bloch, Nature **448**, 1029 (2007).
[4] S. Zöllner, H.-D. Meyer, and P. Schmelcher, Phys. Rev. Lett. **100**, 040401 (2008).
[5] S. Zöllner, H.-D. Meyer, and P. Schmelcher, Phys. Rev. A **78**, 013621 (2008).
[6] J. Li, Y. Yu, A. M. Dudarev, and Q. Niu, New J. Phys. **8**, 154 (2006).
[7] M. Wouters, J. Tempere, and J. T. Devreese, Phys. Rev. A **70**, 013616 (2004).
[8] Ali A. Shams and Henry R. Glyde, Phys. Rev. B **79**, 214508 (2009).
[9] A. Saito, A. Kawakami, H. Shimakage, H. Terai, and Z. Wang, J. Appl. Phys. **92**, 7369 (2002).
[10] J.-Q. Liang, J.-L. Liu, W.-D. Li, and Z.-J. Li, Phys. Rev. A **79**, 033617 (2009).
[11] R. Paredes, Phys. Rev. A **73**, 033616 (2006).
[12] R. A. Barankov and S. N. Burmistrov, Phys. Rev. A **67**, 013611 (2003).
[13] J. Yin, Phys. Rep. **430**, 1 (2006).
[14] F. Gerbier, A. Widera, S. Fölling, O. Mandel, T. Gericke, and I. Bloch, Phys. Rev. A **72**, 053606 (2005).
[15] K. P. Schmidt, J. Dorier, A. Läuchli, and F. Mila, Phys. Rev. B **74**, 174508 (2006).
[16] X.-F. Zhou, Y.-S. Zhang, and G. C. Guo, Phys. Rev. A **80**, 013605 (2009).
[17] R. A. Barankov, C. Lannert, and S. Vishveshwara, Phys. Rev. A **75**, 063622 (2007).
[18] O. Gygi, H. G. Katzgraber, M. Troyer, S. Wessel, and G. G. Batrouni, Phys. Rev. A **73**, 063606 (2006).
[19] P. B. Blakie and W.-X. Wang, Phys. Rev. A **76**, 053620 (2007).
[20] G.-D. Lin, W. Zhang, and L.-M. Duan, Phys. Rev. A **77**, 043626 (2008).
[21] D. Jaksch, C. Bruder, J. I. Cirac, C. W. Gardiner, and P. Zoller, Phys. Rev. Lett. **81**, 3108 (1998).
[22] E. Timmermans, P. Tommasini, M. Hussein, and A. Kerman, Phys. Rep. **315**, 199 (1999).
[23] J. L. DuBois and H. R. Glyde, Phys. Rev. A **63**, 023602 (2001).
[24] A. R. Sakhel, J. L. DuBois and H. R. Glyde, Phys. Rev. A **66**, 063610 (2002).
[25] D.-S. Lühmann, K. Bongs, K. Sengstock, and D. Pfannkuche, Phys. Rev. A **77**, 023620 (2008).
[26] S. R. Clark and D. Jaksch, New J. Phys. **8**, 160 (2006).
[27] M. Capello, F. Becca, M. Fabrizio, and S. Sorella, Phys. Rev. Lett. **99**, 056402 (2007).
[28] B. Capogrosso-Sansone, E. Kozik, N. Prokof'ev, and B. Svistunov, Phys. Rev. A **75**, 013619 (2007).
[29] M. Yamashita and M. W. Jack, Phys. Rev. A **76**, 023606 (2007).
[30] Y. V. Bludov, J. Santhanam, V. M. Kenkre, and V. V. Konotop, Phys. Rev. A **74**, 043620 (2006).
[31] K. Rodriguez, S. R. Manmana, M. Rigol, R. M. Noack, and A. Muramatsu, New J. Phys. **8**, 169 (2006).
[32] I. Titvinidze, M. Snoek, and W. Hofstetter, Phys. Rev. Lett. **100**, 100401 (2008).
[33] F. Hébert, G. G. Batrouni, X. Roy, and V. G. Rousseau, Phys. Rev. B **78**, 184505 (2008).
[34] G.-P. Zheng, J.-Q. Liang, and W. M. Liu, Phys. Rev. A **71**, 053608 (2005).
[35] G.-R. Jin, C. K. Kim, and K. Nahm, Phys. Rev. A **72**, 045601 (2005).
[36] H. Heiselberg, Phys. Rev. A **74**, 033608 (2006).
[37] B. B. Baizakov, B. A. Malomed, and M. Salerno, Phys. Rev. E **74**, 066615 (2006).
[38] V. V. Konotop and M. Salerno, Phys. Rev. A **65**, 021602(R) (2002).
[39] P. Buonsante, R. Franzosi, and V. Penna, J. Phys. B **37**, S195 (2004).
[40] M. Rigol and A. Muramatsu, Phys. Rev. A **69**, 053612 (2004).
[41] E. Burovski, N. Prokof'ev, B. Svistunov, and M. Troyer, New J. Phys. **8**, 153 (2006).
[42] N. V. Prokof'ev, B. V. Svistunov, I. S. Tupitsyn, Phys. Lett. A **238**, 253 (1998).
[43] N. Proko'fev, B. Svistunov, and I. Tupitsyn, Phys. Rev. Lett. **82**, 5092 (1999).
[44] J. E. Cuervo, P.-N. Roy, and M. Boninsegni, J. Chem. Phys. **122**, 114504 (2005).
[45] A. Sarsa, K. E. Schmidt, and W. R. Margo, J. Chem. Phys. **113**, 1366 (2000).
[46] M. H. Kalos and P. A. Whitlock, *Monte Carlo Methods, Volume I: Basics* (John Wiley & Sons, New York, 1986).
[47] E. Merzbacher, *Quantum Mechanics*, 3rd ed. (John Wiley & Sons, New York, 1998).
[48] W. H. Press, S. A. Teukolsky, W. T. Vetterling, and B. P. Flannery, *Numerical Recipes in C*, 2nd ed. (Cambridge University Press, Cambridge, UK, 1999).
[49] A. R. Sakhel, J. L. DuBois, and H. R. Glyde, Phys. Rev. A **77**, 043627 (2008).
[50] T. Giamarchi and H. J. Schultz, Phys. Rev. B **37**, 325 (1988).
[51] O. Morsch and M. Oberthaler, Rev. Mod. Phys. **78**, 179 (2006).
[52] William J. Mullin (private communication).
[53] R. Bach and K. Rzazewski, Phys. Rev. A **70**, 063622 (2004).